Comparison of Noncoherent detectors for SOQPSK and GMSK in Phase Noise Channels

Afzal Syed

Submitted to the Department of Electrical Engineering &
Computer Science and the Faculty of the Graduate School
of the University of Kansas in partial fulfillment of
the requirements for the degree of Master's of Science

Thesis Committee:

_____

Dr. Erik Perrins: Chairperson

_____

Dr. Daniel Deavours

_____

Dr. Glenn Prescott

_____

Date Defended : 2007/08/17

© 2007 Afzal S. Syed

The Thesis Committee for Afzal Syed certifies

That this is the approved version of the following thesis:

Comparison of Noncoherent detectors for SOQPSK and GMSK in Phase Noise Channels

Committee:

_____

Chairperson

_____

_____

_____

Date Approved

To my mother, and to the memory of my father.

Acknowldgements

All praise is due to Almighty Allah.

I thank my mother for giving me the opportunity to study at the University of Kansas, and my father who's always with me. You loved me, inspired me and guided me and I will be ever grateful.

Thank you sister for helping me transition into life in the US and for all the wonderful times. I thank my brother and my brother-in-law for their support and encouragement. I am grateful to Basha uncle and Aunty for giving me valuable advice and for being such amazing people.

I would like to thank my advisor Dr. Perrins, it was an absolute pleasure and a great learning experience working with you. Your knowledge, insight and enthusiasm will always be a source of inspiration for me. Thank you for believing in my ability to complete this work and for your support. I wish to thank Dr. Deavours and Dr. Prescott for being on my committee. Dr. Deavours, thank you for giving me the opportunity to work with you and for helping me on numerous occasions. Your dedication to research is extraordinary. Dr. Prescott, you are among the best teachers that I have had the opportunity to learn from. The two semesters that I worked with you will always be in my memory. I thank Dr. Demarest for encouraging me to be consistently better. I acknowledge the efforts put in by the ITTC staff in making it a center of excellence.

I would like to thank the EECS department for giving me the wonderful experience of being a GTA for three different courses.

I thank all my professors and friends at KU for making my time here memorable and for touching my life in a special way.

Abstract

Shaped offset quadrature phase-shift keying (SOQPSK) and Gaussian minimum shift-keying (GMSK) are highly bandwidth efficient continuous phase modulation (CPM) schemes that are closely related when viewed as OQPSK-type modulations at the receiver. For both of these modulation schemes, coherent detectors are available with good performance in additive white Gaussian noise (AWGN). However in many applications noncoherent receivers are preferred as they are more robust, easy to synchronize and can recover input bits in the presence of phase noise. In this work we provide a comprehensive set of numerical performance results for SOQPSK and GMSK noncoherent detectors in phase noise channels. Since highly bandwidth efficient CPMs such as SOQPSK and GMSK require extremely complex receivers, we also address this problem with several complexity reduction procedures that have been proposed in literature. In particular, these are done for noncoherent detection of GMSK for the first time. We also provide results for serially concatenated (SC)-SOQPSK and SC-GMSK as SC systems with CPM as recursive inner codes have high coding gains at low power and are widely used.

Contents

List of Figures

List of Tables

Chapter 1

Introduction

Communication is one of the most basic needs of mankind and has come a long way since the days of smoke signals. The trend in communication systems has been fast shifting to digital because of the ever-growing demand for data communication and because digital transmission offers data processing options and flexibilities not available with analog transmission. A digital communication system operates using waveforms from a finite set of possible waveforms, differing from an analog communication system which sends a waveform from an infinite variety of waveform shapes with theorically infinite resolution. The objective at the receiver is hence to determine which waveform from the finite set of waveforms was sent by the transmitter from the noisy received signal [39].

Other factors that have led to the digital communications revolution include cheap and highly efficient new hardware, ever increasing service demands, compatilibility and flexibility that digital systems offer and ease of reproduction of digital signals. Digital circuits are more reliable and can be reprogrammed to perform different tasks, they are also less subject to distortion and interference. Encryption and privacy can be easily built into digital systems.

In this work, we study a widely used digital modulation scheme known as continuous phase modulation (CPM). CPM consists of a large family of signals that are especially suited for wireless communication [13] as they achieve high power and bandwidth efficiency. The transmitted signal has a *constant envelope*, i.e. no variations in its amplitude, which is essential in applications using nonlinear amplifiers. Constant envelope modulations are advantageous when simple and inexpensive transmitters are of interest. The power efficiency and signal spectrum of a CPM can be controlled by appropriately choosing the size of the data alphabet, its modulation index, and the frequency pulse.

Constant envelope, power and spectral efficiency are favorable to the *transmitter* and *transmission medium*, however the non linearity of the signal makes it difficult to demodulate and synchronize. Spectral efficiency is often achieved by increasing the size of the data alphabet and by using long and smooth frequency pulses which further increase the complexity of the receiver [27]. Therefore, there is a need to build receivers which are easy to implement with minimal loss in detection efficiency.

In this work we study shaped-offset quadrature phase-shift keying (SOQPSK) and Gaussian minimum shift-keying (GMSK) which are highly bandwidth efficient continuous phase modulation schemes with several desirable qualities. Both of these are MSK-type modulations and are similar to OQPSK [32]. Because of their similary to OQPSK, these modulations can be detected with simple (and suboptimal) OQPSK-type detectors, which is a major motivation for their widespread use. Our interest in these modulations is to compare their performance using noncoherent detectors in phase noise channels. This comparison has not been done before and is important since phase noise channels are often encountered in prac-

2

tice and noncoherent detection is preferred in settings where coherent detection is ineffective. Our results give system designers information that can be used to design future communication standards.

In order to obtain further improvement in energy efficiency and large gains coded systems are used. A class of codes with a multi-stage coding structure whose probability of error decreases exponentially, while decoding complexity increases only linearly were developed by Forney and are known as *concatenated codes* [6]. In this work we also discuss the performance of serially concatenated coded (SCC) noncoherent systems with SOQPSK and GMSK as the inner code and a convolutional code (CC) as the outer code.

SOQPSK has been incorporated into military and aeronautical telemetry standards and it is applicable in any setting where bandwidth-efficient constant-envelope modulations are needed. The version of SOQPSK, that has been part of the MIL-STD 188-181 UHF Satcom standard [1], is known as "MIL-STD SO-QPSK". The version of SOQPSK which has a longer frequency pulse (and hence more bandwith efficient) used by the telemetry group is known as "SOQPSK-TG" [30].

GMSK can achieve a tradeoff among bandwith efficiency, power efficiency, and detector complexity by appropriately configuring the bandwidth-time BT product [15, 44]. The narrow spectral occupancy and rapid side-lobe roll-off provided by the GMSK signal make it an attractive signaling format to use in frequency division multiple access (FDMA) communication systems where total system bandwidth is constrained and adjacent channel interference needs to be minimized. Binary GMSK signals of moderate bandwidth efficiency are implemented in commercial wireless systems, it has been adopted as the modulation scheme for digital

European cordless telecommunications (DECT), global system for mobile communications (GSM) [2,40], and the cordless telephone-second generation (CT-2) [16]. Binary GMSK signals of higher bandwidth efficiency have been adopted in the design of future military satellite communication systems [25].

1.1 Motivation for this thesis and previous work

Since SOQPSK and GMSK are widely used in modern digital communication systems and there has not been much published about how they perform in phase noise, this work quantifies performance of noncoherent detectors for these modulation schemes in such channels for coded and uncoded systems. We compare SOQPSK and GMSK noncoherent detectors' performance in channels with moderate to severe phase noise and give recommmendations on which of these modulation schemes is a better alternative for a given requirment.

In order to build an efficient noncoherent detector, we need to start with the existing optimal coherent detector. The optimal maximum likelihood sequence detection (MLSD) scheme, which is implemented via the Viterbi algorithm (VA), suffers from high complexity in terms of the required number of trellis states and matched filters (MF). A number of techniques have been developed that address this problem, Svensson, Sundberg and Aulin [4] proposed a detector based on a simpler CPM scheme than the one used in the trasmitter. This is known as the pulse truncation (PT) technique and it truncates the frequency pulse to a shorter length, thereby reducing the number of trellis states and MFs simultaneously. Other approaches to reduce the number of MFs use a set of orthonormal basis functions [19], sampling functions [36], Walsh functions [43], and spaced sinusoids [19]. Previous work on reducing the number of trellis states includes

a reduced search algorithm [37] on the full trellis, use of decision feedback on a smaller trellis [14, 41]. The pulse amplitude modulation (PAM) representation of CPM which was introduced by Laurent [23] who showed that a CPM scheme can be represented by a superposition of PAM waveforms is a popular complexity reduction approach and has received a lot of attention in literature.

The complexity reduction techniques for detectors that we use in this work include the PT approach and decision feedback for reducing the number of trellis states. PT for SOQPSK-TG was used in [29] and resulted in a complexity reduction by a factor of 128 with a performance loss of just 0.2 dB. It is used for GMSK with $BT = 0.25$ in this work, we also use decision feedback for updating phase states in the GMSK trellis for the first time.

There has been extensive work done on noncoherent detection schemes, however most of the existing noncoherent detectors use extremely complex metric computations and are difficult to implement in digital hardware. Also, most of the available noncoherent detection algorithms are not applicable to coded systems as discussed in [8]. Colavolpe and Raheli describe a noncoherent sequence estimation which *linearizes* the CPM using Laurent's decomposition in [10]. They also present algorithms applicable to iterative processing, fading and ISI channels in [9]. Though these algorithms have been proven to be efficient in presence of strong phase noise, they are computationally complex and only applicable to simple modulations.

Howlader and Luo consider noncoherent detection of SCC MSK in [18] using exponential windowing for updating phase states. Exponential windowing results in considerable complexity reduction but this algorithm still requires a lot of computational resources as it calculates Bessel functions for each trellis branch.

The other drawback with it is that it cannot be used in log domain for the *soft input soft output* (SISO) algorithm in Chapter 7.

Building on ideas from [22,34] a simple *heuristic* noncoherent detection scheme with performance close to that of coherent detection at moderate phase noise was used in [21] for SOQPSK systems. It is developed here for the first time in coded and uncoded GMSK systems with phase noise.

After the introduction of turbo codes in 1993 [7] there has been a lot of research in the area of concatenated convolutional codes separated by a pseudorandom bit interleaver and decoded iteratively. An *a posteriori* probability (APP) module for iterative decoding of concatenated codes was proposed by Benedetto *et al.* in [5] and this led to the enormous popularity of concatenated codes. Serially concatenated coded systems with CPM as *inner* code have been qualitavely analyzed in [26]. Iteratative decoding for coded OQPSK and SOQPSK was first studied in [24], reduced complexity detection for coded SOQPSK was later described in [27,29]. Coded GMSK systems have been studied in [35], we study the reduced complexity designs and performance of coded GMSK (with $BT = 0.3, 0.25$) for the first time in this work.

Noncoherent detection in SCC systems with iterative detection is a recent development, this work compares the peformance of coded SOQPSK and GMSK systems in channels with phase noise for the first time.

1.2 Outline for the chapters that follow

In Chapter 2 we look at the general CPM signal model and at the more specific signal models for SOQPSK and GMSK. We also discuss the SOQPSK precoders which set it apart from ordinary CPM. In Chapter 3 we present the traditional

optimal maximum likelihood sequence detector (MLSD) for CPM which serves as the benchmark detector for what follows. We discuss optimal and reduced complexity coherent detectors for SOQPSK and look at analytical and simulated results. Coherent detectors for GMSK are studied in Chapter 4.

We discuss a noncoherent detection algortithm that can be used in both coded and uncoded systems in Chapter 5. We also look at performance of noncoherent detectors for SOQPSK and GMSK in AWGN. In Chapter 6 we present a simple phase noise model with varying carrier phase and investigate the performance of noncoherent detectors for SOQPSK and GMSK in phase noise channels for uncoded systems.

Chapter 7 discusses serially concatenated coded systems with iterative decoding. We present the SISO algorithm along with the reduced complexity CPM SISO which is used in SCC systems. We then look at the noncoherent SOQPSK and GMSK performance in SCC systems with phase noise. Finally, we offer conclusions in Chapter 8.

1.3 Paper Publication

This thesis is partly based on the following publication:

A. Syed and E. Perrins, "Comparision of Noncoherent Detectors for SOQPSK and GMSK in Phase Noise Channels", to appear in *Proceedings of the International Telemetering Conference (ITC)*, Las Vegas, NV, October 22-25, 2007.

Chapter 2

Signal Models

In this chapter we start by developing the general CPM signal model and then discuss the specific cases for SOQPSK and GMSK.

2.1 General CPM signal model

We will use complex-baseband notation to represent the various signals. All CPM signals can be described as [3]

$$s(t; \boldsymbol{\alpha}) = \sqrt{\frac{E}{T}} \exp\left\{ j\psi(t; \boldsymbol{\alpha}) \right\} \tag{2.1}$$

where E is the symbol energy, T is the symbol duration, and $\psi(\cdot)$ is the phase of the signal. The information in a CPM signal is carried in its phase which is given by

$$\psi(t; \boldsymbol{\alpha}) \triangleq 2\pi h \sum_{i=-\infty}^{n} \alpha_i q(t - iT), \qquad nT \leq t < (n+1)T \tag{2.2}$$

where h is the *modulation index*, $\boldsymbol{\alpha} = \{\alpha_i\}$ are the data symbols drawn from an M-ary alphabet, and $q(t)$ is the phase pulse. We assume that the modulation

index is a rational number of the form [38]

$$h \triangleq 2K/p. \tag{2.3}$$

The phase pulse $q(t)$ is usually thought of as the time-integral of a *frequency pulse* $f(t)$ with area $1/2$ and duration LT and is given by

$$q(t) \triangleq \begin{cases} 0 & t < 0 \\ \displaystyle\int_0^t f(\tau)\,d\tau & 0 \le t < LT \\ 1/2 & t \ge LT. \end{cases} \tag{2.4}$$

When $L = 1$ the signal is said to be *full response* and when $L > 1$ it is said to be *partial response.* We consider both types of signals in this work.

Considering that the modulation index is a rational number and that $q(t)$ has variations only in the finite interval $(0, LT)$, the phase signal (2.2) can be written as

$$\psi(t; \boldsymbol{\alpha}) = \theta(t; \boldsymbol{\alpha_n}) + \theta_{n-L}. \tag{2.5}$$

The first of these terms is the *correlative phase* and is defined as

$$\theta(t; \boldsymbol{\alpha_n}) \triangleq 2\pi h \sum_{i=n-L+1}^{n} \alpha_i q(t - iT) \tag{2.6}$$

which is a function of the *correlative state vector*

$$\boldsymbol{\alpha_n} \triangleq \alpha_{n-L+1}, \cdots, \alpha_{n-1}, \alpha_n. \tag{2.7}$$

The correlative state vector contains the L most recent data symbols from (2.2)

9

and is drawn from an alphabet of M^L values. To obtain the second term in (2.5) we manipulate the expression

$$\theta_{n-L} \triangleq \pi h \sum_{i=-\infty}^{n-L} \alpha_i \tag{2.8}$$

which contains the remainder of the data symbols from (2.2). θ_{n-L} is known as the *phase state*. Inspite of being a function of an infinite number of data symbols, (2.8) assumes only p unique values when taken modulo-2π due to the rational modulation index assumption. It can also be replaced by the modulo-p look-up table when the table is indexed by the *phase state index* I_{n-L}.

This means that the CPM signal in (2.1) can be described using a trellis with a finite number of states (a finite state machine) with input variable α_n and the L-tuple state vector given by

$$S_n = (\theta_{n-L}, \alpha_{n-L+1}, \cdots, \alpha_{n-2}, \alpha_{n-1}) \tag{2.9}$$

and each branch of the trellis can be defined uniquely by the $(L+1)$-tuple

$$\sigma_n = (\theta_{n-L}, \alpha_{n-L+1}, \cdots, \alpha_{n-2}, \alpha_{n-1}, \alpha_n). \tag{2.10}$$

Hence, the number of states required to describe the CPM signal in (2.2) is [3,33]

$$N_S = pM^{L-1}. \tag{2.11}$$

2.2 Signal Model for SOQPSK

The SOQPSK signal can be compactly defined using (2.1).

For SOQPSK, α_i is drawn from a ternary alphabet, i.e $\alpha_i \in \{-1, 0, +1\}$, where $M = 3$. The modulation index is $h = 1/2$. In this work we discuss two versions of SOQPSK, SOQPSK-MIL [1], which is full response $(L = 1)$ with a rectangular shaped frequency pulse

$$
f_{\mathrm{MIL}}(t) = \begin{cases} \frac{1}{2T}, & 0 \le t < T \\ 0, & \text{otherwise.} \end{cases} \tag{2.12}
$$

The second, SOQPSK-TG [17, 30], is partial-response with $L = 8$ and has a frequency pulse given by

$$
f_{\mathrm{TG}}(t) \triangleq A \frac{\cos(\frac{\pi \rho B t}{2T})}{1 - 4(\frac{\rho B t}{2T})^2} \times \frac{\sin(\frac{\pi B t}{2T})}{\frac{\pi B t}{2T}} \times w(t) \tag{2.13}
$$

where the window is

$$
w(t) \triangleq \begin{cases} 1, & 0 \le |\frac{t}{2T}| < T_1 \\ \frac{1}{2} + \frac{1}{2}\cos(\frac{\pi}{T_2}(\frac{t}{2T} - T_1)), & T_1 \le |\frac{t}{2T}| \le T_1 + T_2 \\ 0, & T_1 + T_2 < |\frac{t}{2T}|. \end{cases} \tag{2.14}
$$

The constant A is chosen such that the area of the pulse is equal to $1/2$ and $T_1 = 1.5$, $T_2 = 0.5$, $\rho = 0.7$ and $B = 1.25$. Figure 2.1 shows the frequency pulse $f_{\mathrm{TG}}(t)$ and corresponding phase pulse $q_{\mathrm{TG}}(t)$.

2.3 SOQPSK precoders

SOQPSK is different from ordinary CPM in that ternary data are the output of a precoder as shown in Figure 2.2. There are two commonly used precoders for
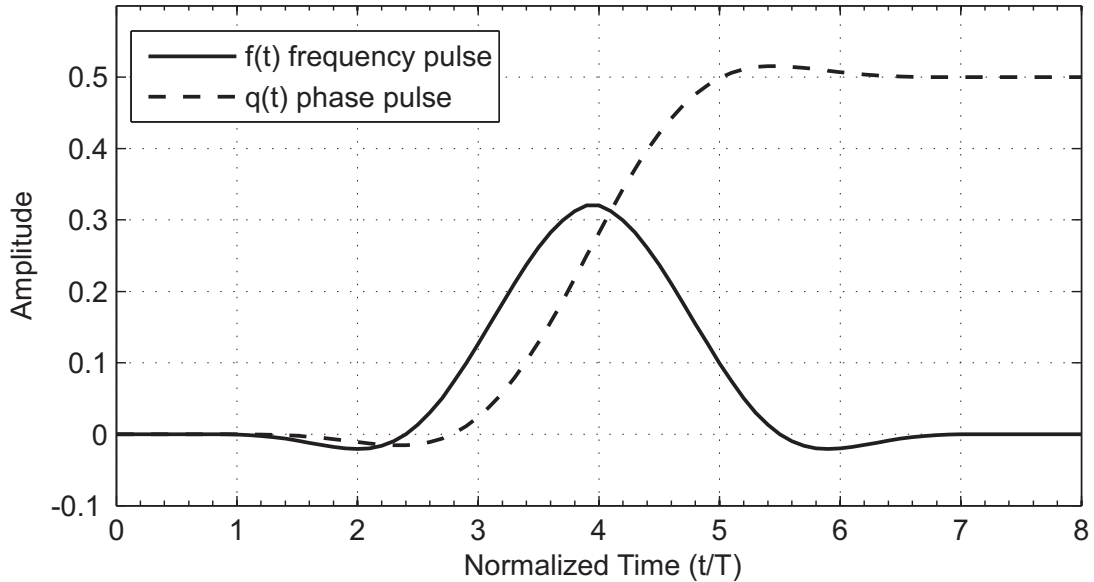
Figure 2.1. The length-8T frequency and phase pulses for SOQPSK-TG.

SOQPSK.

2.3.1 Standard SOQPSK precoder

The standard precoder converts binary data $a_n \in \{0, 1\}$ into ternary data α_i according to the mapping [38]

$$\alpha_n = (-1)^{n+1}(2a_{n-1} - 1)(a_n - a_{n-2}). \tag{2.15}$$
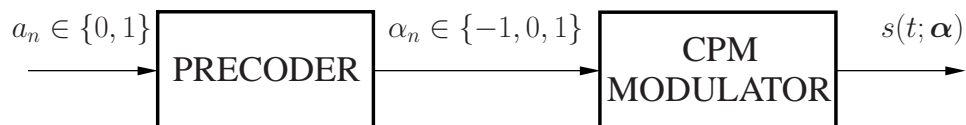
Figure 2.2. Signal model for uncoded SOQPSK.

The original motivation for SOQPSK was that (2.15) leads to a simple (but

suboptimal) symbol-by-symbol detection architecture [11]. The precoder orients the phase of the CPM signal in (2.2) such that it behaves like the phase of an OQPSK signal that is driven by the bit sequence a_i, the inphase and quadrature bits can thus be recovered using a standard OQPSK detector. The precoder *undoes* the infinite phase response of the CPM modulator, i.e the phase state in (2.8), which in turn allows the simple symbol-by-symbol detection architecture. In this work, we seek trellis based optimal detectors for the system in Figure 2.2.

The SOQPSK precoder in (2.15) imposes three important constraints on the ternary data [38]:

1. While α_i is viewed as being *ternary*, in any given symbol interval α_i is actually drawn from one of two *binary* alphabets, $\{0, +1\}$ or $\{0, -1\}$.

2. When $\alpha_i = 0$, the binary alphabet for α_{i+1} switches from the one used for α_i, when $\alpha_i \neq 0$ the binary alphabet for α_{i+1} does not change.

3. A value of $\alpha_i = +1$ cannot be followed by $\alpha_{i+1} = -1$, and vice versa (this is implied by the previous constraint).

2.3.2 Recursive SOQPSK precoder

Another useful precoder for SOQPSK that satisfies the constraints described above can be obtained by differentially encoding the original bits a_n at the transmitter. The differential (recursive) nature of this alternate precoder formulation is essential when SOQPSK is used as the inner code in a serially concatenated system [6] to realize coding gains. The differentially encoded bits are

$$d_n = a_n \oplus d_{n-2} \qquad (2.16)$$

where $\oplus$ is the XOR operator for binary data in the set $\{0, 1\}$. The precoder in this case is

$$\alpha_n = (-1)^n a_n d'_{n-1} d'_{n-2} \tag{2.17}$$

where $d'_n \in \{-1, 1\}$ is the antipodal counterpart of d_n and is given by $d'_n = 2d_n - 1$. Although shown in equation form in (2.17), this recursive precoder is the same as the one shown as a block diagram in [24, Fig. 7]. This is the precoder we use for all the SOQPSK systems discussed in this work as differential encoding is enabled for noncoherent detection of SOQPSK.

2.4 Signal Model for GMSK

GMSK is a popular form of CPM [3] and is also compactly defined by (2.1). The frequency pulse $f(t)$ for GMSK is given by

$$f(t) = \frac{1}{2T} \left\{ Q \left[2\pi B \frac{t - T/2}{(\ln 2)^{1/2}} \right] - Q \left[2\pi B \frac{t + T/2}{(\ln 2)^{1/2}} \right] \right\} \tag{2.18}$$

where the parameter B is chosen to obtain desired distance or spectral properties [3] and

$$Q(t) = \frac{1}{\sqrt{2\pi}} \int_t^\infty e^{-\tau^2/2} \, d\tau. \tag{2.19}$$

In this work we use GMSK with $BT = 0.3$ and $BT = 0.25$. The reason for choosing these particular cases of BT products is that the performance of GMSK with $BT = 0.25$ in AWGN is very close to that of SOQPSK-TG and GMSK with $BT = 0.3$ is a widely used for several applications. We also use the same complexity reduction technique i.e frequency pulse truncation [42] for SOQPSK-TG and GMSK with $BT = 0.25$. This allows us to better compare their
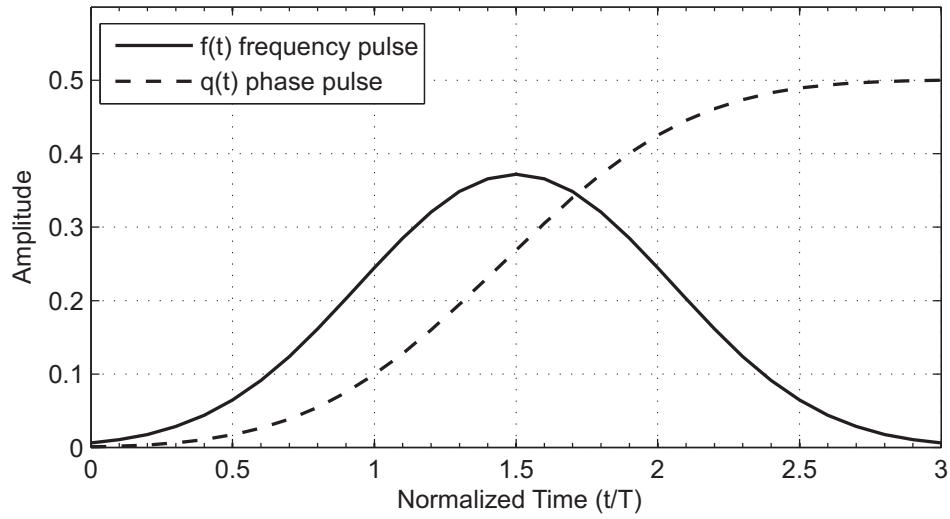
Figure 2.3. The length-3T frequency and phase pulses for GMSK with $BT = 0.3$.

performance in phase noise and coded systems.

GMSK is binary $(M = 2)$ and has a modulation index $h = \frac{1}{2}$. For the case when $BT = 0.3$, the signal is partial response with $L = 3$, Figure 2.3 shows the frequency pulse $f(t)$ and corresponding phase pulse $q(t)$.
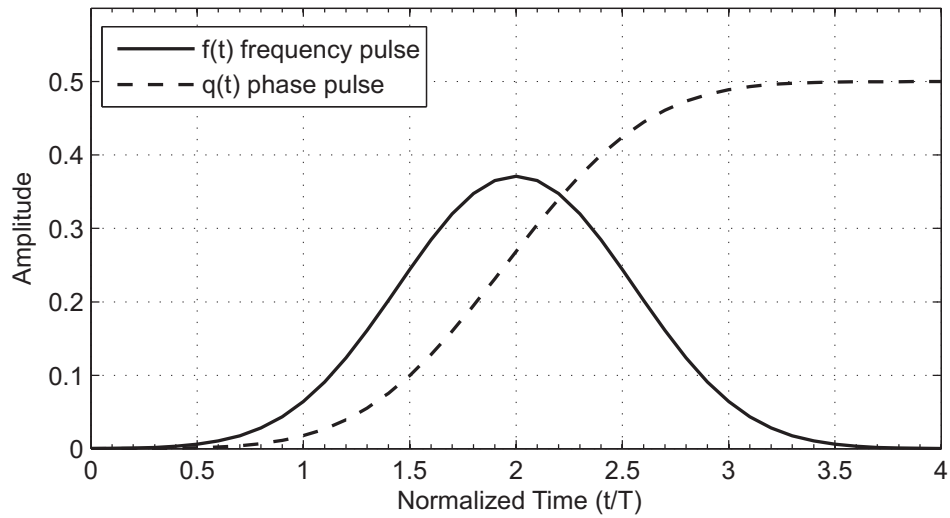
Figure 2.4. The length-4T frequency and phase pulses for GMSK with $BT = 0.25$.

An ever more bandwith efficient signal results when $BT = 0.25$, this is also partial response with $L = 4$. Figure 2.4 shows $f(t)$ and $g(t)$ for GMSK with $BT = 0.25$.

2.5 Comparison of Power Spectral Densities
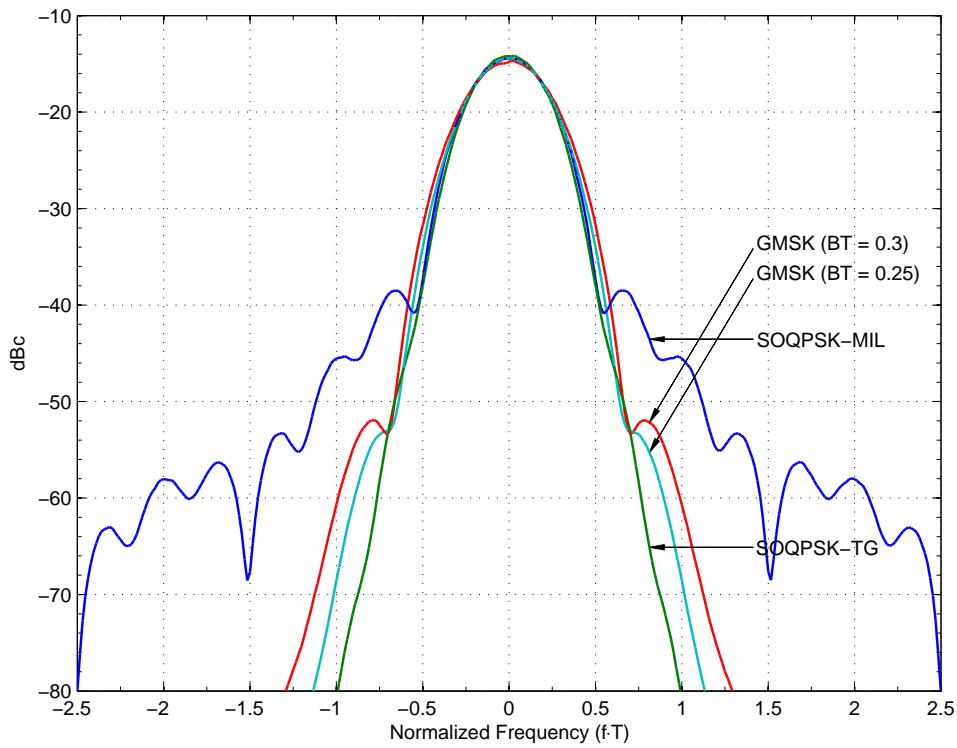
Figure 2.5. Power spectral densities for SOQPSK and GMSK

Figure 2.5 shows the power spectral densities for SOQPSK and GMSK. The amplitude is dB relative to an unmodulated carrier (dBc). It can be observed that SOQPSK-*TG* is the most bandwidth efficient and GMSK ($BT = 0.25$) is slightly more bandwith efficient when compared to GMSK ($BT = 0.3$)

Now that we have defined all the required signal models, we can start building receivers for these modulation schemes.

Chapter 3

Coherent Detectors for SOQPSK

Although our objective is to arrive at noncoherent detectors for SOQPSK and GMSK, we will first examine optimal coherent detectors. This will yield models upon which the noncoherent detectors will be built. In this chapter we start with a discussion of optimal coherent maximum likelihood detectors for CPM, then we build coherent detectors for SOQPSK-*MIL* and SOQPSK-*TG*.

3.1 Optimal Coherent ML Detectors for CPM

A maximum likelihood (ML) reciever is that receiver which selects the most likely signal sent, given a waveform $r(t)$ that it has observed [3]. We discuss an ML receiver for a signaling waveform sent through additive white Gaussian noise, the AWGN channel. In what follows, we refer to the estimated and hypothesized values of a generic quantity a as $\hat{a}$ and $\tilde{a}$ respectively. Also, $\hat{a}$ and $\tilde{a}$ can assume the same values as a itself.

The received signal is

$$r(t) = s(t; \boldsymbol{\alpha}) + n(t) \tag{3.1}$$

where $n(t)$ is a complex valued AWGN process with one-sided power spectral density N_0. The log-likelihood function for (3.1), given a hypothetical data sequence $\tilde{\boldsymbol{\alpha}}$, is [27]

$$\Lambda(\tilde{\boldsymbol{\alpha}}) = -\int_{-\infty}^{\infty} |r(t) - s(t; \tilde{\boldsymbol{\alpha}})|^2 \, dt. \tag{3.2}$$

The maximum likelihood sequence detector (MLSD) finds the sequence $\tilde{\boldsymbol{\alpha}}$ that maximizes (3.2). As $s(t; \tilde{\boldsymbol{\alpha}})$ is constant envelope, maximizing (3.2) is equivalent to maximizing the correlation [3]

$$\lambda(\tilde{\boldsymbol{\alpha}}) = \text{Re} \int_{-\infty}^{\infty} r(t) s^*(t; \tilde{\boldsymbol{\alpha}}) \, dt \tag{3.3}$$

where $(\cdot)^*$ represents the complex conjugate.

A reciever based on these calculations is called a *correlation receiver*. The Viterbi Algorithm (VA) can be used to efficiently compute (3.3). The following is the organization of the trellis which contains pM^L branches. Each *branch vector* is the $(L+1)$-tuple

$$\sigma_n \triangleq (\theta_{n-L}, \alpha_{n-L+1}, \cdots, \alpha_{n-1}, \alpha_n) \tag{3.4}$$

$$= (\theta_{n-L}, \boldsymbol{\alpha_n}) \tag{3.5}$$

which can be represented equivalently, as a phase state index and a correlative state vector as in (3.5). Each branch has a *starting state*

$$S_n = (\theta_{n-L}, \alpha_{n-L+1}, \cdots, \alpha_{n-1}) \tag{3.6}$$

18

and an ending state

$$E_n = (\theta_{n-L+1}, \alpha_{n-L+2}, \cdots, \alpha_{n-1}, \alpha_n). \tag{3.7}$$

Using these definitions, (3.3) can be computed recursively by [3]

$$\lambda_{n+1}(\tilde{E}_n) = \lambda_n(\tilde{S}_n) + \mathrm{Re}\{(e^{-j\theta_{n-L}} z_n(\tilde{\boldsymbol{\alpha}_n}))\} \tag{3.8}$$

where $\lambda_n(\cdot)$ is the *cumulative metric* for a given state at index n and $z_n(\tilde{\boldsymbol{\alpha}_n})$ is a sampled matched filter output

$$z_n(\tilde{\boldsymbol{\alpha}_n}) \triangleq \int_{nT}^{(n+1)T} r(t) e^{-j\psi(t;\tilde{\boldsymbol{\alpha}_n})} \, dt \tag{3.9}$$

which is one symbol interval's worth of correlation in (3.3) [27]. Using (3.9) in (3.8) the increment for the *cumulative metric* is given by

$$\mathrm{Re}\left\{ e^{-j\theta_{n-L}} \int_{nT}^{(n+1)T} r(t) e^{-j\psi(t;\tilde{\boldsymbol{\alpha}})} \, dt \right\}. \tag{3.10}$$

The implementation of the receiver can be described using (3.10). This is shown in Figure 3.1. The received signal is fed to the bank of *matched filters* (MFs). The MFs are based on the correlative phase $\theta(\cdot)$ and produce M^L complex-valued outputs, one for each possible value of the correlative state vector. The MF bank can be constructed with [3]

$$N_{MF} = M^L \tag{3.11}$$

real-valued MFs. The set of M^L MF outputs are then rotated by the p phase
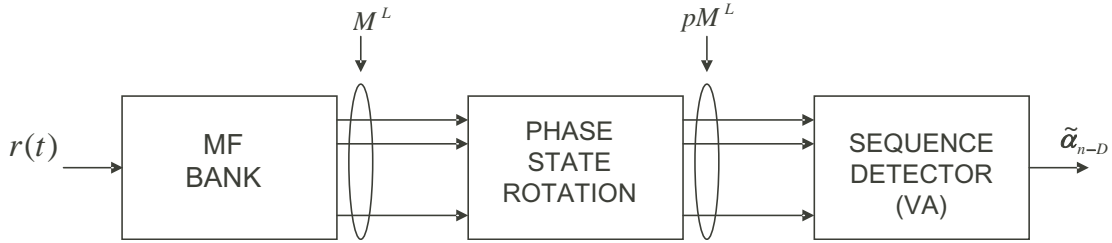
Figure 3.1. Optimal CPM detector.

states, resulting in pM^L real-valued inputs to the VA [27]. Then it's just the matter of implementing the VA, each ending state E_n has M possible metrics. As M branches merge into each ending state of the trellis, there are M candidate values for $\lambda_{n+1}(\tilde{E}_n)$. At each ending state, the VA declares a *local survivor*, which is the branch with the maximum metric. The identity of each local survivor is stored in a *traceback matrix* for decoding later on. The state with the maximum overall metric at the end of n-th symbol interval is called the *global survivor*. The VA traces back along the sequence of local survivors which precede the global survivor to a sufficient length known as the *traceback length*(TB). The VA then outputs a reliable decision at this delayed point in time, the decision being the data associated with the surviving branch at $\hat{S}_{n-TB}$. The local suvivors, global survivors, and other values stored in the traceback matrix are used a number of times in the noncoherent detector.

3.2 Coherent Detection Algorithm for Full-Response SOQPSK

The precoder in (2.17) can be described with an 8-state trellis, with three binary-valued state variables : n-even/n-odd, a_{n-1} and a_{n-2}. If we construct a *time-varying* trellis, with different sections for n-even and n-odd, then we have
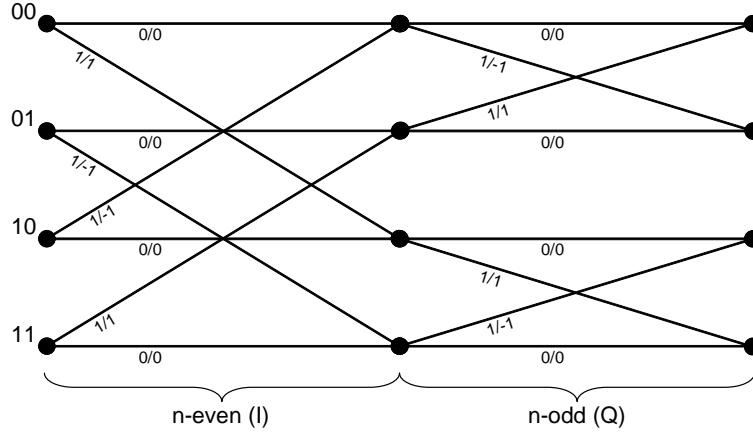
Figure 3.2. 4-state time-varying trellis for the precoder/CPM Modulator. The labels along the branches are for the input bit/output symbol pair a_n/α_n.

the 4 state trellis shown in Figure 3.2. The labels along each branch show the input bit/output symbol pair, a_n/α_n, for the given branch. The state variables are a_{n-1}, and a_{n-2} and are ordered such that the inphase bit of this pair is always the MSB and the quadrature bit of this pair is always the LSB. When n is even, the branch bit a_n replaces the inphase bit in the state variable, and likewise for the quadrature bit when n is odd. Thus for n-even, the state variables are ordered (a_{n-2}, a_{n-1}) and for n-odd the ordering is (a_{n-1}, a_{n-2}). Each state in Figure 3.2 is labeled with a unique value of $S_n \in \{00, 01, 10, 11\}$, and so the branches can be described as

$$\sigma_n = (S_n, a_n). \tag{3.12}$$

There is a one-to-one mapping between the trellis state values, in the set $\{00, 01, 10, 11\}$, and the CPM phase states which is shown in Figure 3.3. It is evident that the CPM phase states are a $\pi/4$-rotated version of the traditional QPSK constellation.

21
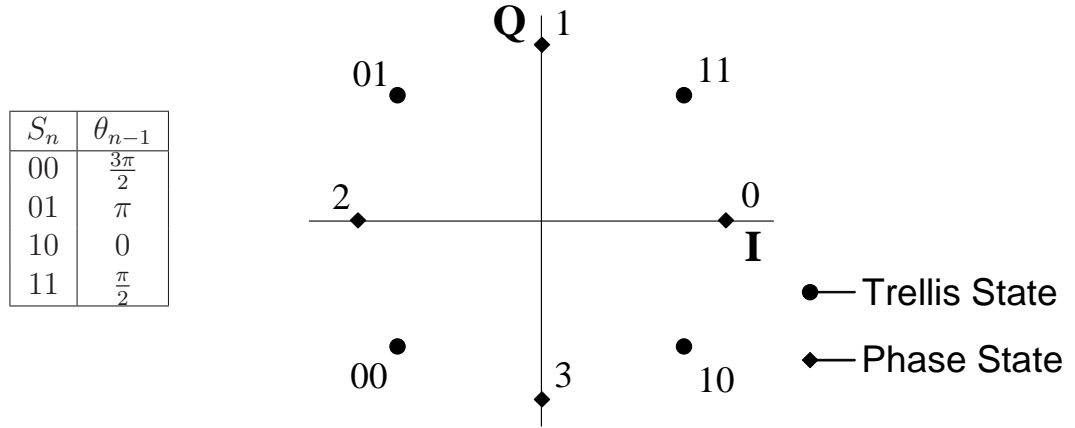
Figure 3.3. The mapping between the trellis states and the phase state index.

With the trellis defined for the system in Figure 2.2, we outline the optimal detector for the received signal (3.1). SOQPSK-MIL being full-response, no additional states are required and an optimal maximum likelihood sequence detection (MLSD) detector can be obtained from this 4-state trellis [24] using the Viterbi algorithm discussed in the previous section. Using (3.8) the recursive metric update for this specific case is given by

$$\lambda_{n+1}(\tilde{E}_n) \triangleq \lambda_n(\tilde{S}_n) + \mathrm{Re}\{e^{-j\tilde{\theta}_{n-1}} z_n(\tilde{\alpha}_n)\} \tag{3.13}$$

where $\lambda_n(\cdot)$ is the cumulative metric for a given state at index n and $z_n(\tilde{\alpha}_n)$ is a sampled matched filter output given by

$$z_n(\tilde{\alpha}_n) \triangleq \int_{nT}^{(n+1)T} r(t) e^{-j2\pi h\tilde{\alpha}_n q(t-nT)} \, dt. \tag{3.14}$$

As two branches merge into each ending state in Figure 3.2, there are two candidate values for $\lambda_{n+1}(\tilde{E}_n)$. The VA is used to find the output symbols.

3.3 Detection of Partial-Response SOQPSK-TG

After defining the optimal *coherent* detector for *full*-response SOQPSK, we can look at the modifications needed to arrive at the *coherent* detector for *partial*-response SOQPSK.

An optimal detector for the TG version of SOQPSK optimal detector requires $p \cdot 2^{L-1}$ or 512 phase states due to the partial-response of the waveform. Instead of using the optimal detector with a 512-state trellis we pursue a near-optimum approximation for SOPQPSK-TG. The appromixation method we use is frequency pulse truncation (PT) [42] which is based on the 4-state trellis in Figure 3.2 with a loss in performance of 0.2 dB. This minor loss is attractive in light of the large reduction in the number of trellis states.

The PT approach stems from the fact that frequency pulses which are long and smooth are oftentimes near zero for a significant portion of their duration. This is clearly the case for $f_{TG}(\text{t})$ in Figure 2.1. We base the detector on a frequency pulse which has been truncated to a duration of one symbol time(full-response). Since the detector uses a *phase* pulse, we translate these arguments accordingly and obtain a modified phase pulse

$$q_{PT}(t) = \begin{cases} 0, & t < 0 \\ q(t + (L-1)T/2), & 0 \le t \le T \\ 1/2, & t > T. \end{cases} \qquad (3.15)$$

Even though the phase pulse in (3.15) has infinite duration, its time-varying portion has been shortened to the interval $[0, T]$ as shown in Figure 3.4, which gives it full-response behavior. Now, it can be used with the 4-state trellis in

23
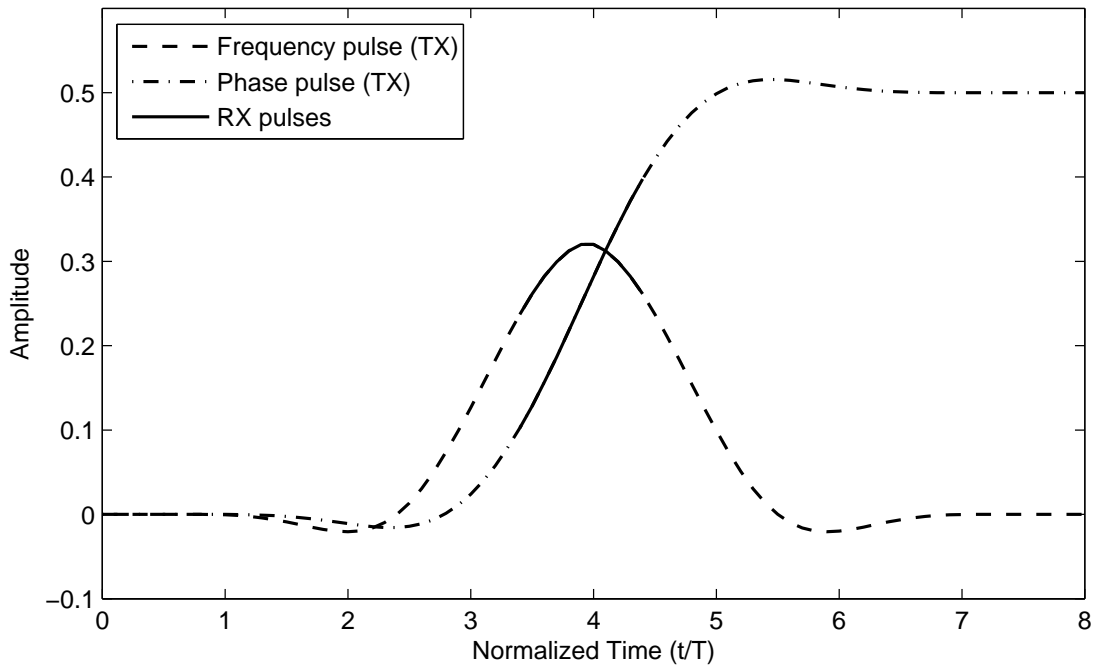
Figure 3.4. Truncated frequency and phase pulse for SOQPSK-TG.

Figure 3.2 and in the full-responce CPM metric (3.14), which serves as the branch metric increment for the Viterbi algorithm in (3.13).

3.4 Performance

The error performance of SOQPSK in additive white Gaussian noise is described using error events and minimum distance concepts as discussed in [29]. The normalized squared Euclidean distance of CPM is [3]

$$d^2 = \frac{\log_2 M_{\text{info}}}{2T} \int |s(t; \alpha_{Tx}) - s(t; \alpha_{Rx})|^2 dt \qquad (3.16)$$

where $\log_2 M_{\text{info}}$ is the number of bits per symbol (for SOQPSK we have $M_{\text{info}} = 2$). Using union bound the probability of bit error for uncoded SOQPSK-MIL and
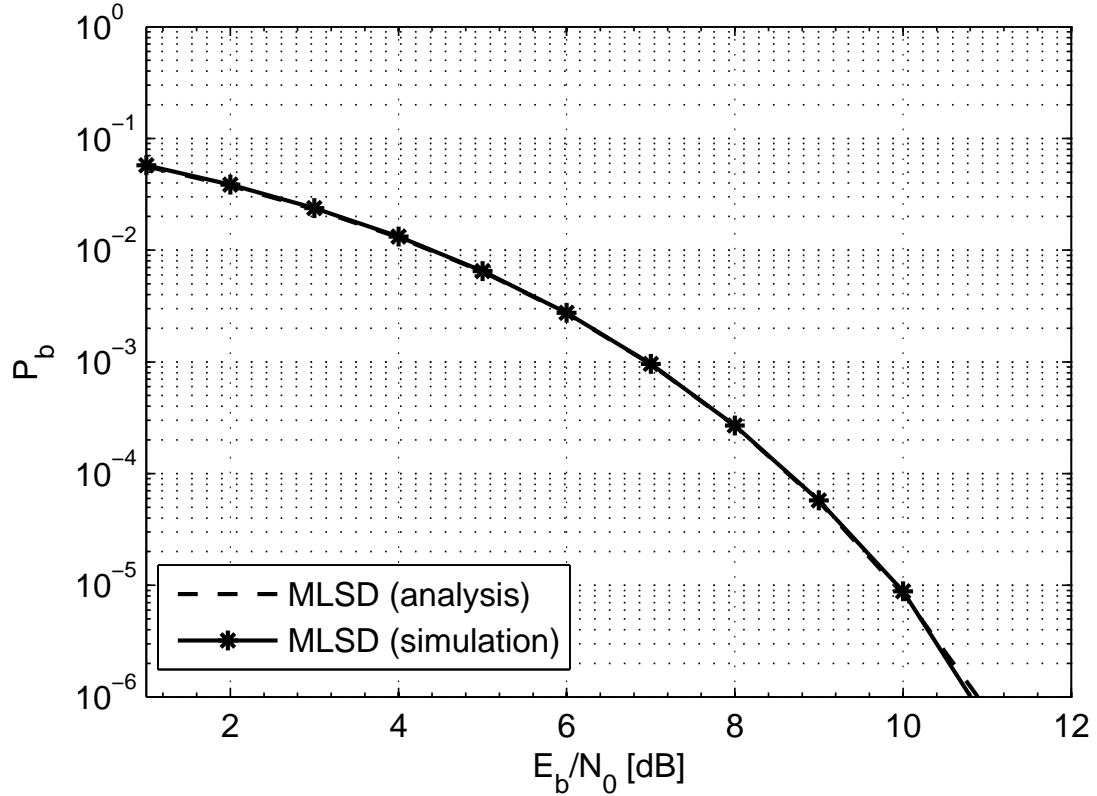
Figure 3.5. Performance of Optimal Coherent Detector for SOQPSK-MIL.

SOQPSK-TG using the 4-state time variant trellis is found to be bounded-by

$$P_b \leq Q\left(\sqrt{d_0^2 \frac{E_b}{N_0}}\right) + Q\left(\sqrt{d_1^2 \frac{E_b}{N_0}}\right) \tag{3.17}$$

where E_b/N_0 is the bit energy to noise ratio and $Q(t)$ is the Q function given by (2.19)

For SOQPSK-MIL $d_0^2 = 1.73$ [3] and $d_1^2 = 2.36$. For SOQPSK-TG we have $d_0^2 = 1.60$ and $d_1^2 = 2.59$. Figures 3.5 and 3.6 and show the theoretical and simulated curves for SOQPSK-MIL and SOQPSK-TG using pulse truncation. It can be observed that the PT approximation results in a loss of only 0.2 dB which agrees with the analysis and simulation published in [29].
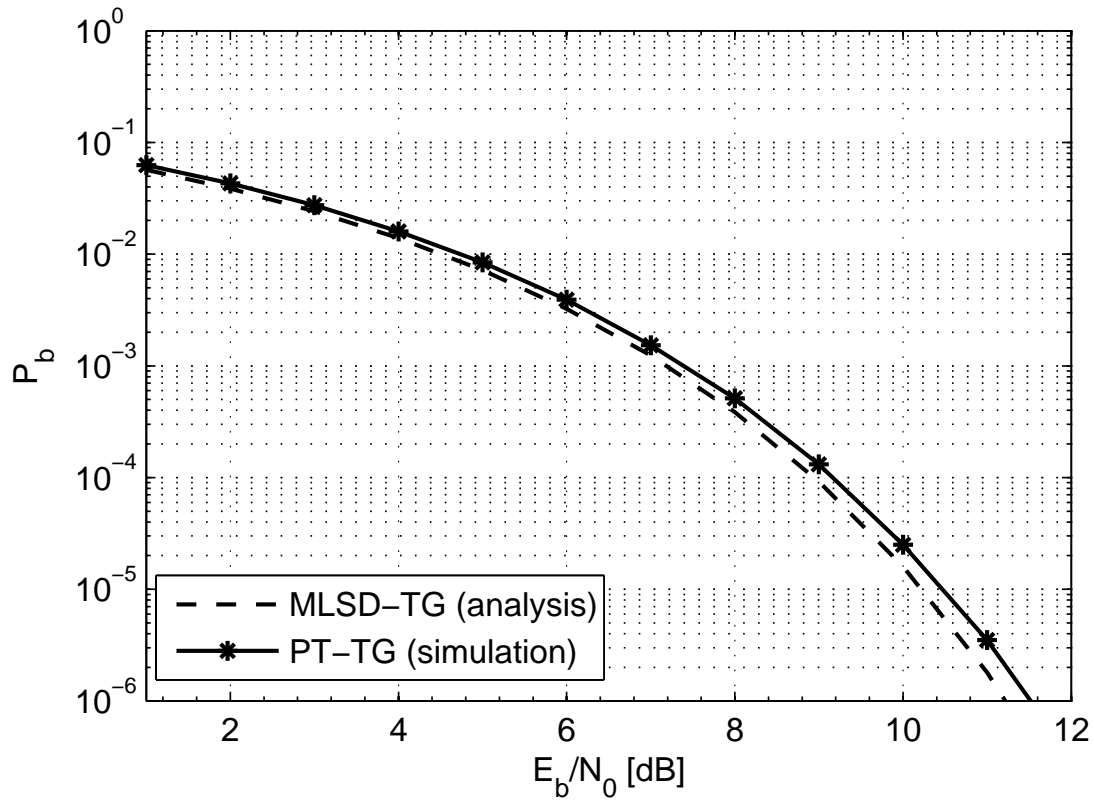
Figure 3.6. Performance of Reduced Complexity Coherent Detector for SOQPSK-TG.

Differential encoding produces two bit errors for each detection error, hence the bit error performance of SOQPSK systems without differential encoding would be (3.17) scaled by a factor of $\frac{1}{2}$. At $P_b = 10^{-5}$, the scale factor translates to a 0.3 dB advantage for a system without differential encoding. However, this advantage approaches zero asymptotically as E_b/N_0 increases.

Chapter 4

Coherent Optimal and Reduced

Complexity Detectors for GMSK

We discuss the optimal coherent detector models for GMSK with $BT = 0.3$ and $BT = 0.25$ in this chapter. Then we build reduced complexity detectors which use a much smaller trellis for the first time.

4.1 Optimal detectors for GMSK

Starting with the information carrying phase in (2.2), for h and $f(t)$ for any symbol interval n, the phase $\psi(t, \boldsymbol{\alpha})$ is defined by $\boldsymbol{\alpha_n}$, the correlative state vector $(\alpha_{n-L+1}, \cdots, \alpha_{n-2}, \alpha_{n-1})$ and the phase state θ_{n-L}, where

$$\theta_{n-L} = h\pi \sum_{i=-\infty}^{n-L} \alpha_i \bmod 2\pi. \qquad (4.1)$$

The number of correlative states is finite and equal to M^{L-1}. For rational modulation indices, $h = 2k/p$ the phase trellis has p different phase states with values $0, 2\pi/p, 2.2\pi/p, \cdots, (p-1)2\pi/p$. The total state is defined by the

27

L-tuple $\sigma_n = (\theta_{n-L}, \alpha_{n-L+1}, \cdots, \alpha_{n-2}, \alpha_{n-1})$, and the number of such states is $N_s = pM^{L-1}$.

The number of matched filters required would be M^L as outlined in section 3.1 and given by

$$\text{MF}(\boldsymbol{\alpha_n}) \triangleq \exp(-j2\pi h \sum_{i=n-L+1}^{n} \alpha_i q(t - nT_s)), \quad 0 \leq t < LT_s \qquad (4.2)$$

where $\tilde{\boldsymbol{\alpha}}_n$ is given by the L-tuple $(\alpha_{n-L+1}, \cdots, \alpha_{n-2}, \alpha_{n-1}, \alpha_n)$ and T_s denotes one symbol time. These properties are used in receiver structures for any CPM.

4.1.1 GMSK with $BT = 0.3$

GMSK with $BT = 0.3$ has a frequency pulse with $L = 3$ (Figure 2.3), the modulation index h is $1/2$, the number of phase states p is 4. Using (2.11) we have 16 $(4 \cdot 2^2)$ trellis states defined by the 3-tuple

$$S_n = (\theta_{n-3}, \alpha_{n-2}, \alpha_{n-1}) \qquad (4.3)$$

and the 4 phase states are $0, \pi/2, \pi, 3\pi/2$. This trellis is shown in Figure 4.1. This requires 8 matched filters (as $L = 3$) as given by (4.2) and for this case $\tilde{\boldsymbol{\alpha}}_n$ is defined by $(\alpha_{n-2}, \alpha_{n-1}, \alpha_n)$.

Now that the trellis is set up and the matched filters have been defined, the optimal coherent detector for GMSK is the implementation of the Viterbi algorithm with the recursive metric update (3.13) as detailed in section 3.2.
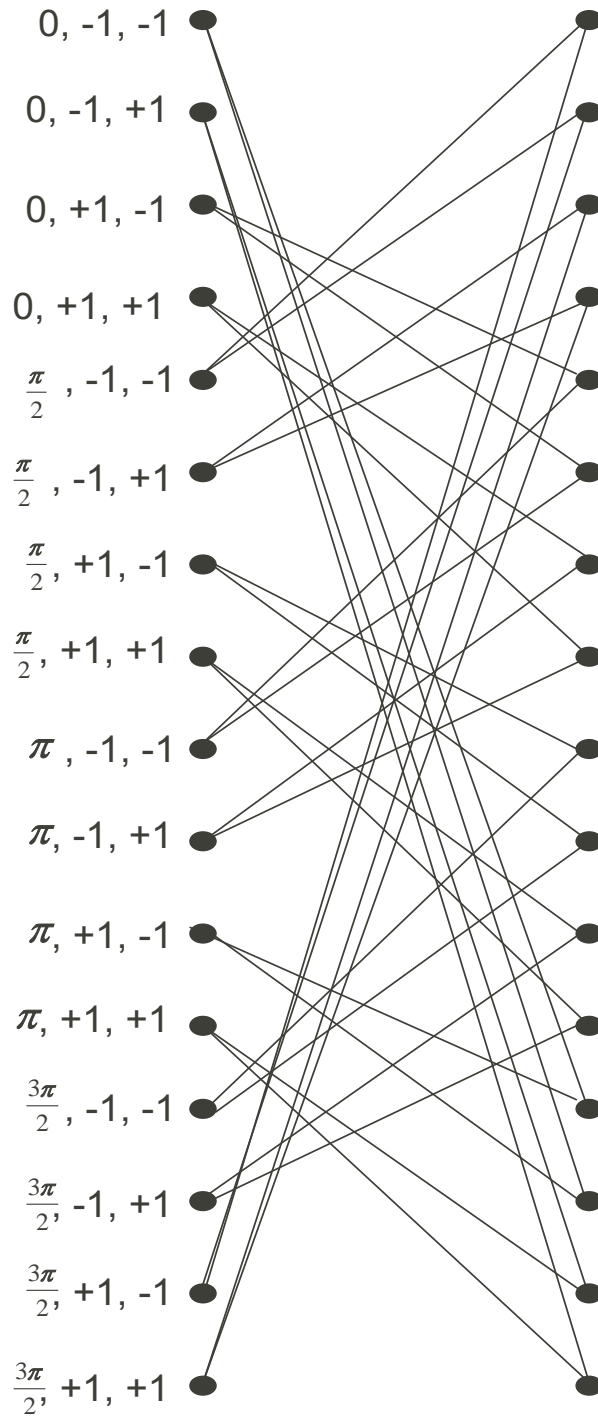
Figure 4.1. GMSK 16 trellis for $BT = 0.3$, $(\theta_{n-3}, \alpha_{n-2}, \alpha_{n-1})$ represent the trellis states. The branches represent the output symbol α_n.

4.1.2 GMSK with $BT = 0.25$

Optimal coherent detection of GMSK with $BT = 0.25$ is very similar to that of GMSK with $BT = 0.3$, but the trellis is larger as the frequency pulse has a longer duration of $L = 4$. Using (2.11) we have 32 $(4 \cdot 2^3)$ trellis states defined by the 4-tuple

$$S_n = (\theta_{n-4}, \alpha_{n-3}, \alpha_{n-2}, \alpha_{n-1}). \tag{4.4}$$

The trellis would be similar to the $BT = 0.3$ trellis shown in Figure 4.1. We would require 16 matched filters (as $L = 4$) as given by (4.2) and for this case $\tilde{\boldsymbol{\alpha}}_{\boldsymbol{n}}$ is defined by $(\alpha_{n-3}, \alpha_{n-2}, \alpha_{n-1}, \alpha_n)$.

The optimal coherent detector with 32 trellis states and 16 matched filters would be difficult to implement so we look for ways to reduce complexity with a minimal loss in performance.

4.2 Reduced complexity detectors for GMSK

In this section we discuss methods to reduce the trellis size to 4 states for each of these GMSK schemes. One of the reasons to use a 4 state for GMSK is to better compare its performance with SOQPSK which has a 4 state trellis.

4.2.1 Complexity reduction for GMSK with $BT = 0.3$

For the 16 state trellis for GMSK with $BT = 0.3$ each branch is defined by $\sigma_n = (\theta_{n-3}, \alpha_n, \alpha_{n-1}, \alpha_{n-2})$ and the trellis states are defined by $S_n = (\theta_{n-3}, \alpha_{n-1}, \alpha_{n-2})$, this can be reduced to a 4 state trellis having the same 8 matched filters by using *decision feedback* [14] to update phase states. For such a trellis the states would be defined as $S_n = (\alpha_{n-2}, \alpha_{n-1})$ and branches as $\sigma_n = (\alpha_{n-2}, \alpha_{n-1}, \alpha_n)$. As can

be observed there is no phase reference in either of the definitions, we store the phase associated with each trellis state and update it at each stage or *time-step* of the trellis using (4.1).

Each trellis state starts off with phase $\theta = 0$ and for each subsequent stage of the trellis the phase is updated using (4.5). There are two branches which end in each trellis state and the branch which has the higher branch metric is the survivor, with symbol $\hat{\alpha}_{n-2}$, the phase state for the hypothesised ending state can then be estimated using

$$\hat{\theta}_{n-2}(\tilde{E}_n) = \hat{\theta}_{n-3}(\tilde{S}_n) + \pi h \tilde{\alpha}_{n-2} \tag{4.5}$$

which is a simplified version of (4.1) for this particular case.
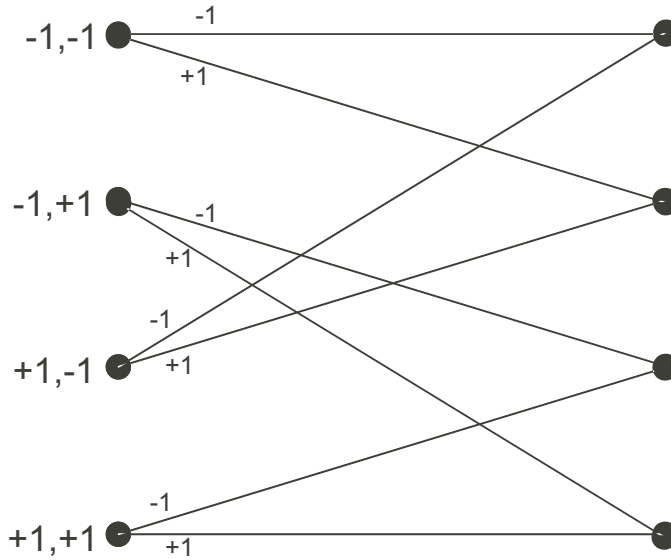
Figure 4.2. GMSK trellis reduced to 4 states, $\alpha_{n-2}, \alpha_{n-1}$ represent the trellis states. The labels along the branch represent the output symbol α_n.

The reduced complexity trellis with just 4 trellis states is showin in Figure 4.2. Since each state has the correlative state vector and a phase state $\hat{\theta}$ associated

with it, we can apply the Viterbi alorithm for coherent detection. This detector would have very close performance as the optimal detector with 16 trellis states as the number of matched filters remain unchanged and we store a matrix of phase states associated with each trellis state and use decision feedback to update it.

4.2.2 Complexity reduction for GMSK with $BT = 0.25$
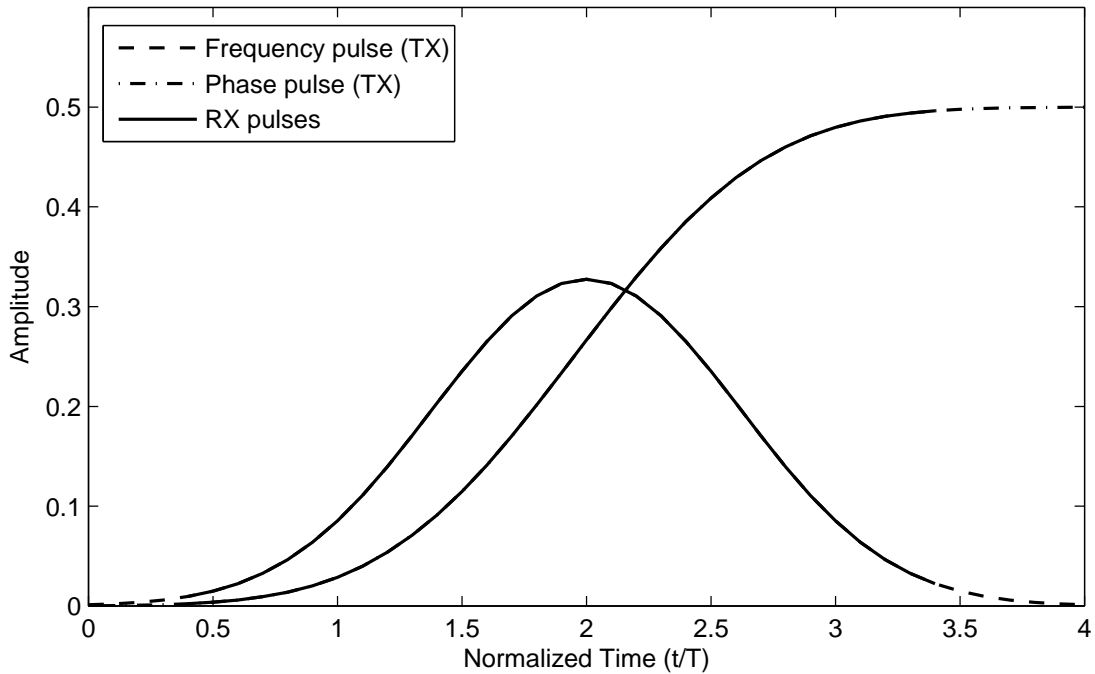
Figure 4.3. Truncated frequency and phase pulses for GMSK with $BT = 0.25$.

We would like to use the same 4 state trellis as above, for GMSK with $BT = 0.25$. Observing that the frequency pulse $f(t)$ in Figure 2.4 is near zero for at least one symbol duration we can use the *pulse truncation* approach outlined in section 3.3 and truncate the frequency pulse at the receiver to a duration of 3 symbol times as shown in Figure 4.3. This reduces the number of trellis states to 16 defined by the 3-tuple $(\theta_{n-3}, \alpha_{n-2}, \alpha_{n-1})$, each branch is defined by

$B_n = (\theta_{n-3}, \alpha_n, \alpha_{n-2}, \alpha_{n-1})$. This is the exact same trellis as in Figure 4.1 for GMSK with $BT = 0.3$. We can follow the same procedure as in the previous section and use decision feedback to reduce it to the 4-state trellis in Figure 4.2.
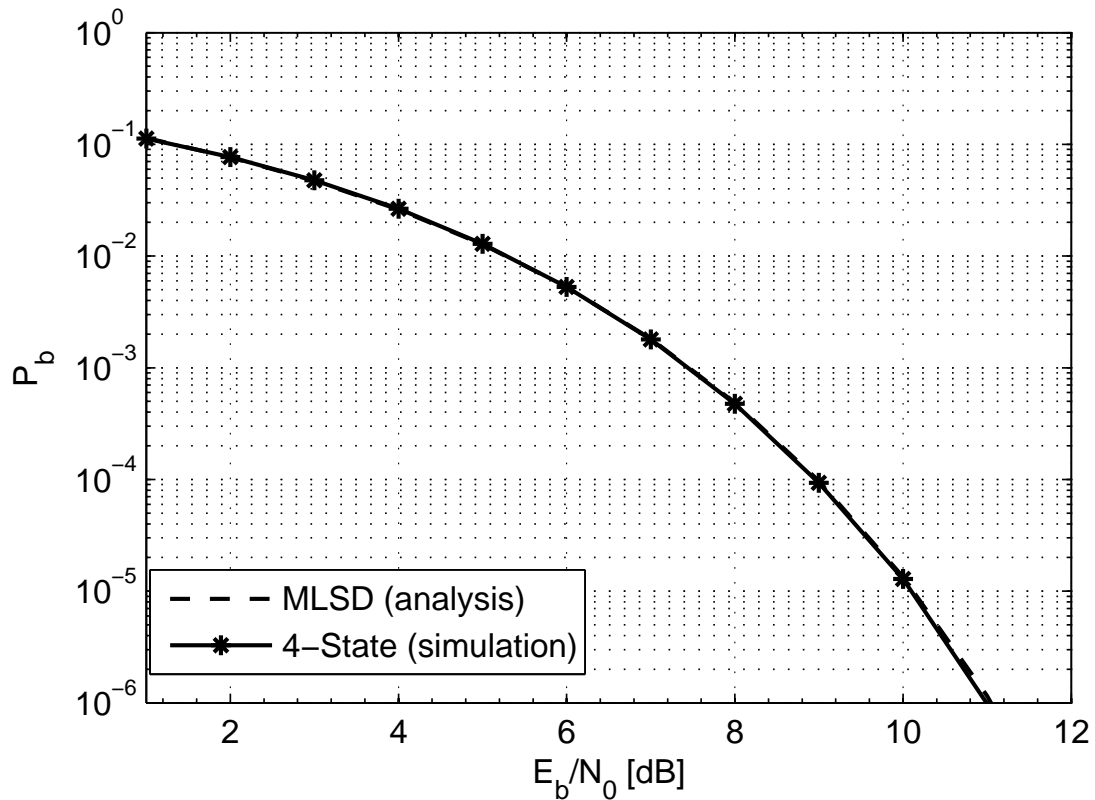
Figure 4.4. Performance of Coherent Detector for GMSK with $BT = 0.3$.

4.3 Performance

The error performance of coherent detectors for GMSK in additive white Gaussian noise can be described using error events and minimum distance concepts as stated in section 3.4. Using union bound the probability of bit error (MLSD) for GMSK is found to be bounded-by
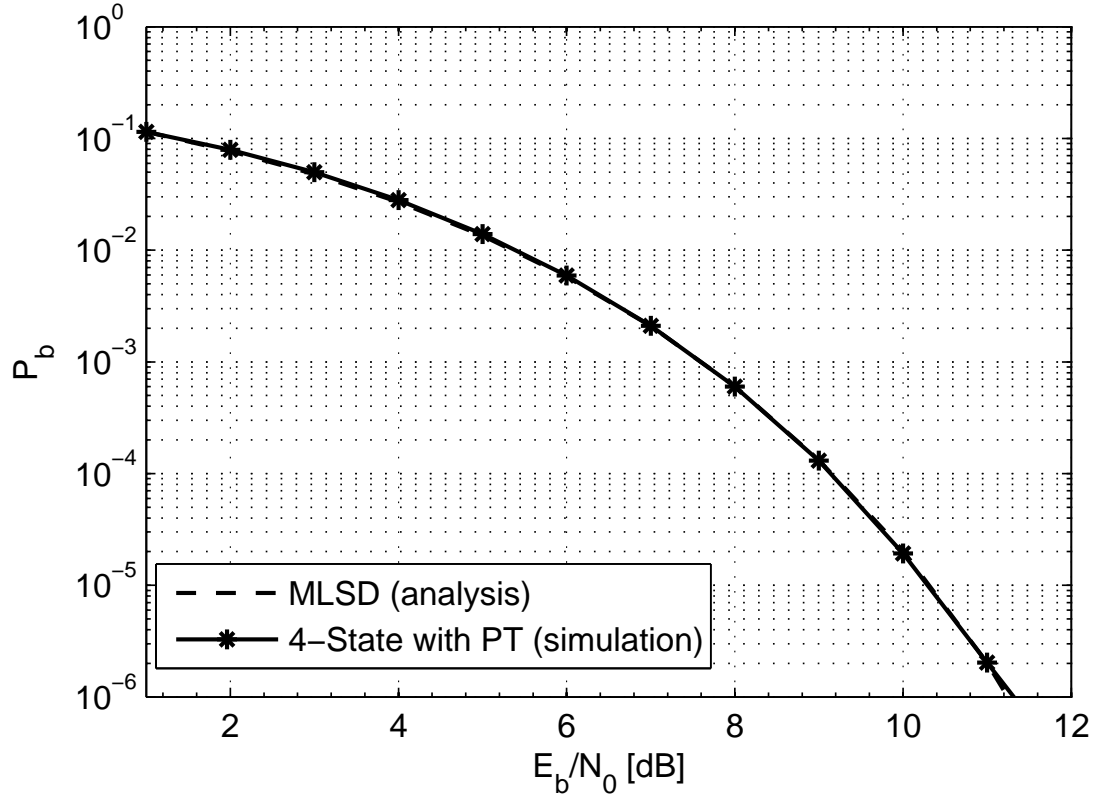
Figure 4.5. Performance of Coherent Detector for GMSK with $BT = 0.25$.

$$P_b \leq Q\left(\sqrt{d_0^2 \frac{E_b}{N_0}}\right) + Q\left(\sqrt{d_1^2 \frac{E_b}{N_0}}\right) \tag{4.6}$$

which is similar to SOQPSK.

For GMSK with $BT = 0.3$, $d_0^2 = 1.78$ and $d_1^2 = 2.26$ and for GMSK with $BT = 0.25$ we have $d_0^2 = 1.69$ and $d_1^2 = 2.37$. Figures 4.4 and 4.5 and show the theoretical and simulated curves for GMSK with $BT = 0.3$ and $BT = 0.25$ respectively. It can be observed that the peformance of reduced complexity detector for $BT = 0.3$ is almost the same as MLSD peformance and the loss in performance for $BT = 0.25$ is less than 0.01 dB.

Chapter 5

Noncoherent Detector models

5.1 Introduction

It is generally assumed that the receiver has complete knowledge of the carrier phase, this requires a phase locked loop (PLL) in the receiver for carrier tracking. Such is detector is called a *coherent detector*, the drawbacks of using coherent detection include expensive hardware, increase in receiver complexity, false locks at low SNR, phase slips, loss of locks due to Doppler shift etc.

Noncoherent detection eliminates the need for PLLs and provides a way to recover the information bits in the presence of *phase noise* [21].

5.2 Noncoherent Detection Algorithm

Now, the model for the received complex-baseband signal is

$$r(t) = s(t, \boldsymbol{\alpha})e^{j\phi(t)} + n(t) \qquad (5.1)$$

the phase shift $\phi(t)$ introduced by the channel is unknown in general, for the moment we assume that it is a constant (but unknown) value of ϕ_0, we consider variations in carrier phase when we study the performance of noncoherent detectors.

Using a similar approach as [22, 34] the cumulative metric for a given state at index n in (3.13) is modified as

$$\lambda_{n+1}(\tilde{E}_n) = \lambda_n(\tilde{S}_n) + \mathrm{Re}\{Q_n^*(\tilde{S}_n)e^{-j\tilde{\theta}_{n-L}}z_n(\tilde{\boldsymbol{\alpha}_n})\} \tag{5.2}$$

where the complexed-valued *phase reference* $Q_n(\cdot)$ is given by the recursive update

$$Q_{n+1}(\tilde{E}_n) \triangleq aQ_n(\tilde{S}_n) + (1-a)e^{-j\tilde{\theta}_{n-L}}z_n(\tilde{\boldsymbol{\alpha}_n}) \tag{5.3}$$

with the *forgetting factor* a being a real number in the range $0 < a < 1$. The forgetting factor a defines the rate at which the older phase estimates are updated.

The phase references are updated after the local surviors at each trellis stage of the Viterbi algorithm are declared.When a is chosen to be close to 1, more weight is assigned to the previous phase reference and the update is done very slowly. This is closer to coherent detection. If a is chosen to be close to 0, phase references are updated at a faster rate and less weight is assigned to its previous values. This algorithm can be used for noncoherent detection of any CPM including SOQPSK (MIL and TG) and GMSK.

5.3 Performance

In this section we look at the performance of noncoherent detectors for SO-QPSK (MIL and TG) and GMSK, in the presence of AWGN only (no phase noise),

(a)

a	loss [dB] at $P_b = 10^{-5}$
0.625	1.65
0.75	1.0
0.875	0.45
1.0	0

Legend:
- a=0.625
- a=0.75
- a=0.875
- a=1 (coherent)
- MLSD

P_b vs E_b/N_0 [dB]

(b)

a	loss [dB] at $P_b = 10^{-5}$
0.625	2.60
0.75	1.60
0.875	0.75
1.0	0.2

Legend:
- a=0.625
- a=0.75
- a=0.875
- a=1 (Coherent)
- MLSD

P_b vs E_b/N_0 [dB]
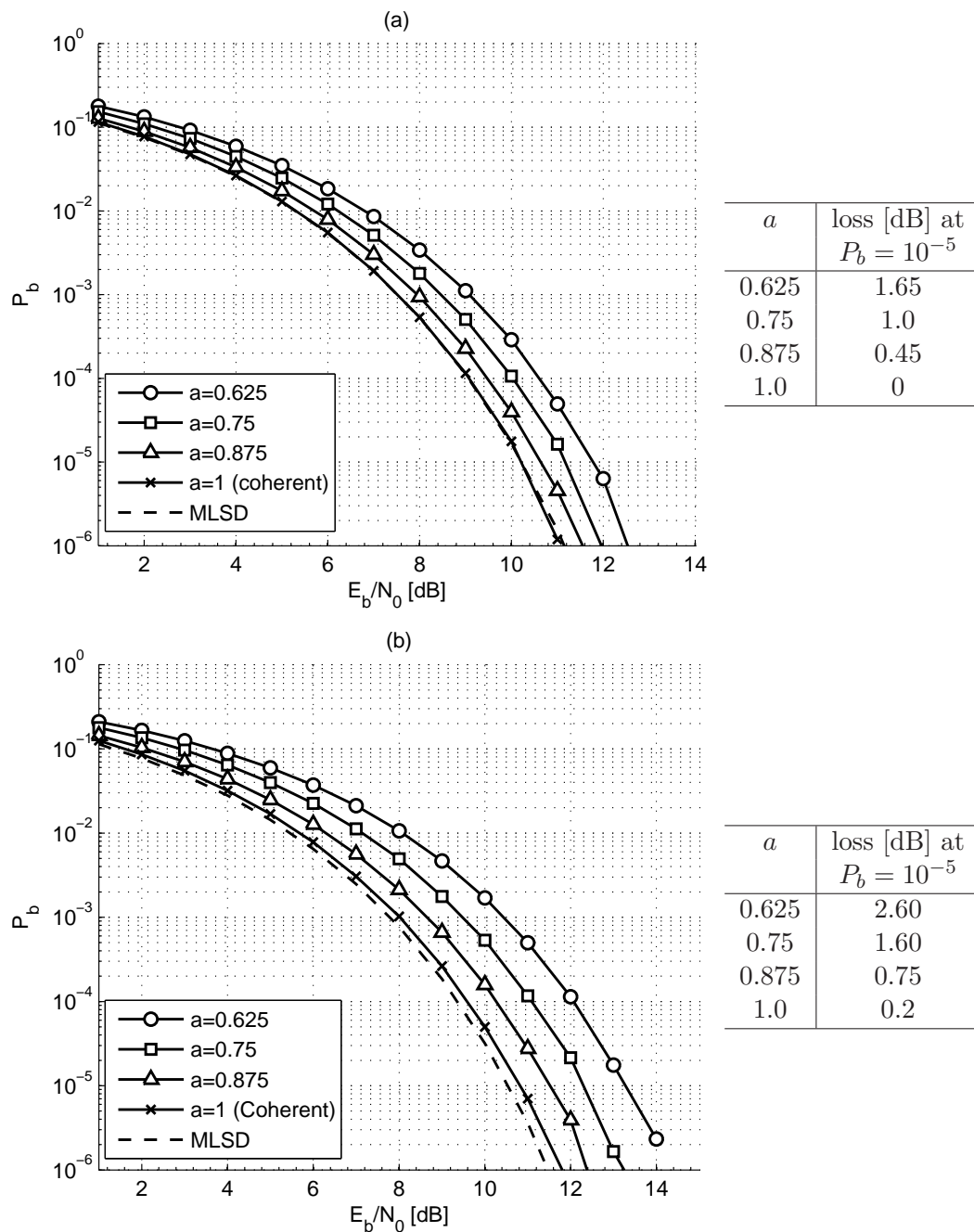
Figure 5.1. Performance of Noncoherent a) SOQPSK-MIL and b) SOQPSK-TG detectors in AWGN (no phase noise) with varying values of a. In the table to the right of the plot, the loss relative to MLSD at $P_b = 10^{-5}$ is quantified for each value of a.

(a)

a	loss [dB] at $P_b = 10^{-5}$
0.625	0.9
0.75	0.65
0.875	0.7
1.0	0

(b)

a	loss [dB] at $P_b = 10^{-5}$
0.625	1.10
0.75	1.0
0.875	0.75
1.0	0
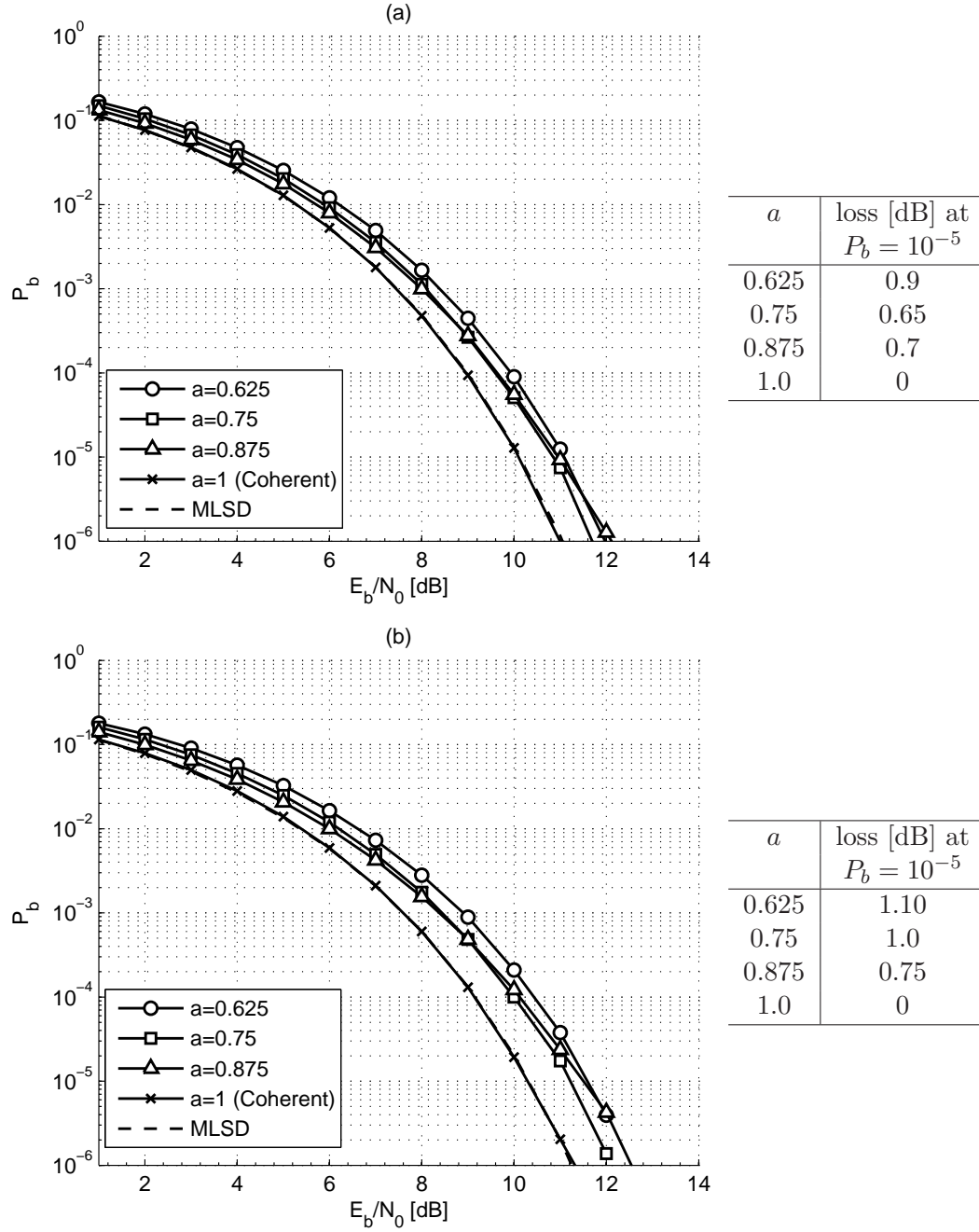
Figure 5.2. Performance of Noncoherent GMSK with a) $BT = 0.3$ and b) $BT = 0.25$ detectors in AWGN (no phase noise) with varying values of a. In the table to the right of the plot, the loss relative to MLSD at $P_b = 10^{-5}$ is quantified for each value of a.

for a few values of the forgetting factor a.

Table 5.1. Loss in dB for noncoherent systems with no phase noise at $P_b = 10^{-5}$.

Modulation Scheme	$a = 1$	$a = 0.875$	$a = 0.75$	$a = 0.625$
SOQPSK-MIL	0	0.45	1	1.65
SOQPSK-TG	0.2	0.75	1.60	2.60
GMSK with $BT = 0.3$	0	0.70	0.65	0.9
GMSK with $BT = 0.25$	0	0.75	1.0	1.1

The forgetting factor a has an unavoidable impact on bit error performance. Unlike PCM/FM in [21], the performance of noncoherent SOQPSK detectors is very sensitive to this value. However, the GMSK noncoherent detectors are not very sensitive to the value of a. Figures 5.1 and 5.2 show the performance of these noncoherent detectors in AWGN only (no phase noise), for varying values of a. The GMSK curves are closer to the MLSD performance when compared to the SOQPSK curves. Table 5.1 summarizes the loss in dB for noncoherent systems with no phase noise as a function of the forgetting factor at $P_b = 10^{-5}$. It can be observed that the loss grows quite large as a decreases.

The demerit of these noncoherent detectors is that they may not be applicable to fading channels [21] since the algorithm tracks only the phase variations and does not use amplitude reference symbols as [18].

Chapter 6

Performance in Phase Noise Channels

6.1 Introduction

This chapter discusses the numerical performance results for SOQPSK-MIL, SOQPSK-TG and GMSK noncoherent detectors. Although we are interested in a non coherent detector, the natural choice for benchmark is optimal coherent maximum likelihood sequence detection (MLSD). The MLSD probability of bit error for differentially encoded SOQPSK-MIL and SOQPSK-TG using the 4-state time variant trellis and for GMSK using the optimum trellis is tightly upper-bounded by

$$P_b \leq Q\left(\sqrt{d_0^2 \frac{E_b}{N_0}}\right) + Q\left(\sqrt{d_1^2 \frac{E_b}{N_0}}\right) \tag{6.1}$$

where E_b/N_0 is the bit-energy-to-noise ratio and $Q(t)$ is the Q function given by (2.19).

As discussed in previous chapters, the values for d_0^2 and d_1^2 for SOQPSK and GMSK are summarized in Table 6.1.

Table 6.1. Error Distances for SOQPSK and GMSK.

Modulation Scheme	d_0^2	d_1^2
SOQPSK-MIL	1.73	2.36
SOQPSK-TG	1.60	2.59
GMSK with $BT = 0.3$	1.78	2.24
GMSK with $BT = 0.25$	1.69	2.37

6.2 Phase Noise Model

Since the motivation for a noncoherent receiver is the case when the carrier phase is not known and assumed to be varying, a simple model will be introduced for variations in the carrier phase. Let [31]

$$\phi_n \equiv \phi(nT) = \phi_{n-1} + \nu_n \bmod 2\pi \qquad (6.2)$$

where $\{\nu_n\}$ are independent and identically distributed Gaussian random variables with zero mean and variance δ^2. This models the phase noise as a first order Markov process with Gaussian transition probability distribution. For perfect carrier phase tracking, $\delta = 0$.

6.3 Performance

Using the phase noise model from above, we present simulated results for performance of noncoherent detectors in this section.

Figures 6.1, 6.2, 6.3 and 6.4 show the performance of noncoherent detectors for SOQPSK and GMSK in phase noise as function of the forgetting factor a,
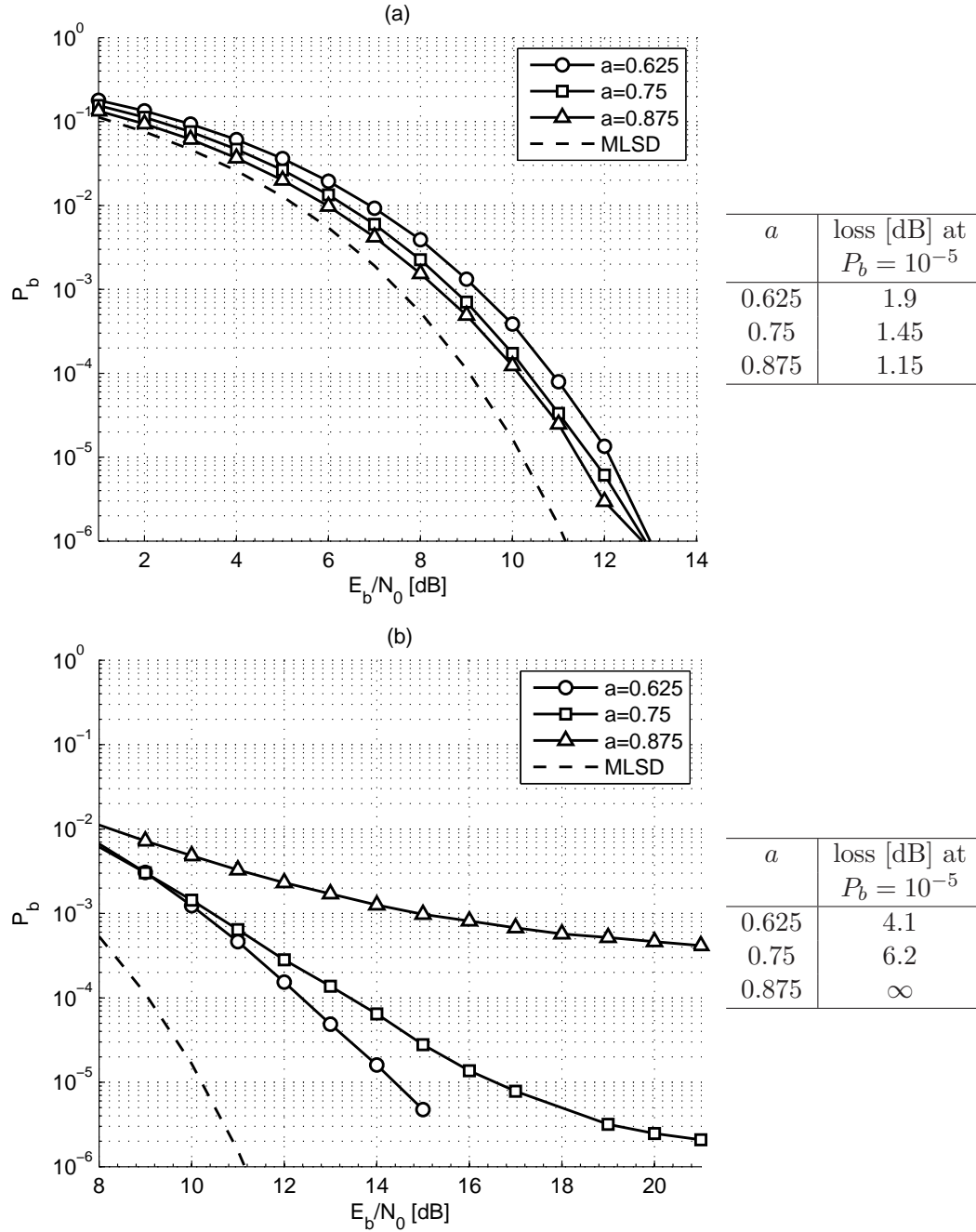
Figure 6.1. Performance of Noncoherent SOQPSK-MIL detector with a) $\delta = 2°$/symbol and b) $\delta = 5°$/symbol. The table to the right of the plot, shows the loss relative to MLSD at $P_b = 10^{-5}$ for each value of a.

(a)

a	loss [dB] at $P_b = 10^{-5}$
0.625	3.1
0.75	2.4
0.875	2.3

(b)

a	loss [dB] at $P_b = 10^{-5}$
0.625	9.8
0.75	∞
0.875	∞
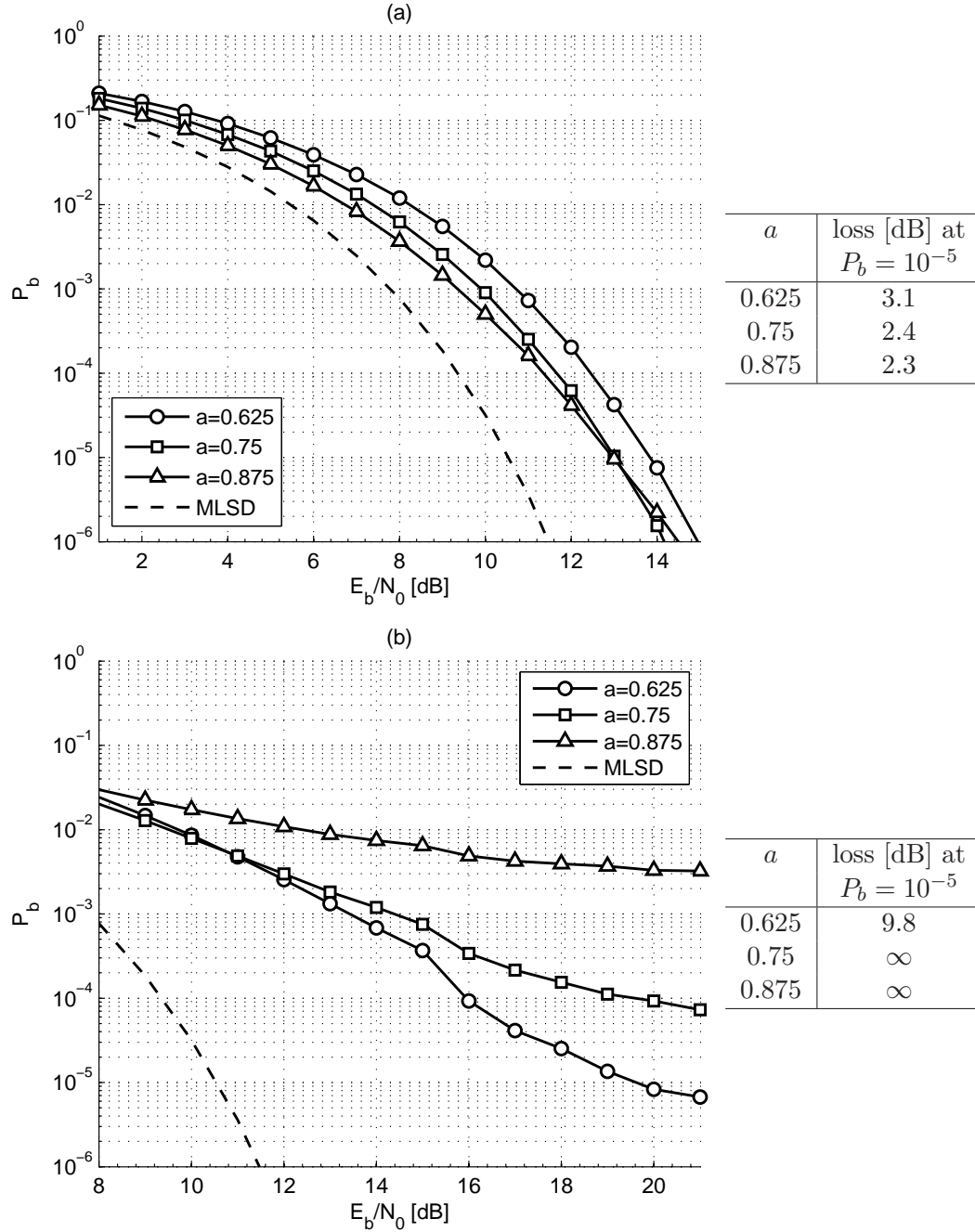
Figure 6.2. Performance of Noncoherent SOQPSK-TG detector with a) $\delta = 2°$/symbol and b) $\delta = 5°$/symbol. The table to the right of the plot, shows the loss relative to MLSD at $P_b = 10^{-5}$ for each value of a.

(a)

a	loss [dB] at $P_b = 10^{-5}$
0.625	1.15
0.75	0.95
0.875	0.9

(b)

a	loss [dB] at $P_b = 10^{-5}$
0.625	2.0
0.75	3.05
0.875	∞
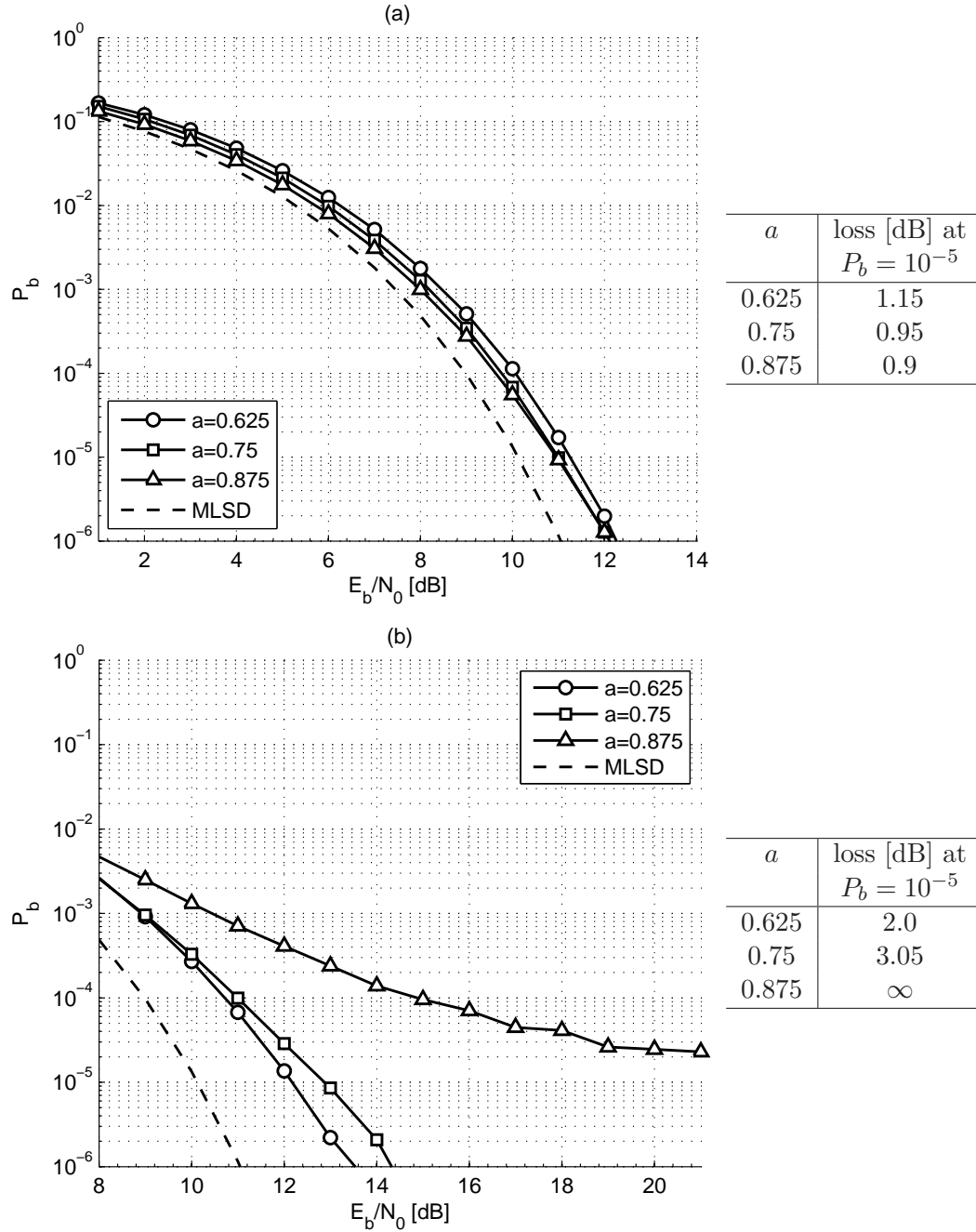
Figure 6.3. Performance of Noncoherent GMSK with $BT = 0.3$ detector with a) $\delta = 2°$/symbol and b) $\delta = 5°$/symbol. The table to the right of the plot, shows the loss relative to MLSD at $P_b = 10^{-5}$ for each value of a.

(a)

a	loss [dB] at $P_b = 10^{-5}$
0.625	1.6
0.75	1.25
0.875	1.2

(b)

a	loss [dB] at $P_b = 10^{-5}$
0.625	2.85
0.75	3.10
0.875	∞
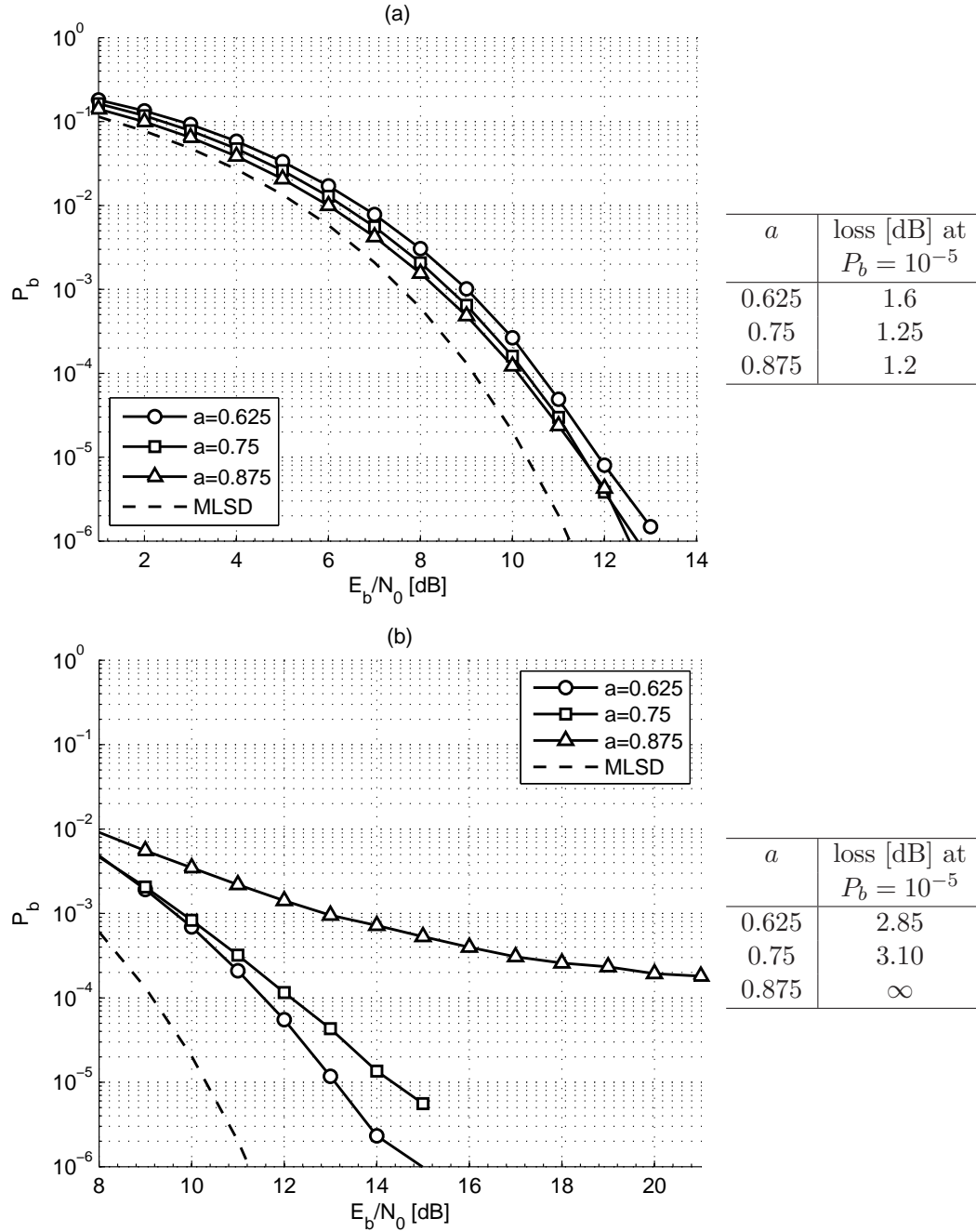
Figure 6.4. Performance of Noncoherent GMSK with $BT = 0.25$ detector with a) $\delta = 2°$/symbol and b) $\delta = 5°$/symbol. The table to the right of the plot, shows the loss relative to MLSD at $P_b = 10^{-5}$ for each value of a.

3 different values of a were chosen to establish a relation between this design paramater and performance. $\delta = 2°$/symbol and $\delta = 5°$/symbol were the 2 values chosen for δ.

Table 6.2. Loss in dB for noncoherent systems with phase noise of $\delta = 2°$/sym. at $P_b = 10^{-5}$.

Modulation Scheme	$a = 0.875$	$a = 0.75$	$a = 0.625$
SOQPSK-MIL	1.15	1.45	1.9
SOQPSK-TG	2.3	2.4	3.1
GMSK with $BT = 0.3$	0.90	0.95	1.15
GMSK with $BT = 0.25$	1.2	1.25	1.6

Table 6.2 summarizes the loss in dB for noncoherent detectors for $\delta = 2°$/symbol. For the moderate value of $\delta = 2°$/symbol, both the SOQPSK-MIL and GMSK noncoherent detectors show similar performance, SOQPSK-TG performs significantly worse. Some of this degradation in performance for noncoherent SOQPSK-TG detector could be attributed to the 0.2 dB [28] loss due to the PT approximation. Also, the loss grows large as a decreases. The best value for a was found to be 0.875. The performance curves for GMSK are relatively close together compared to the SOQPSK curves. The loss measured relative to MLSD at $P_b = 10^{-5}$ for SOQPSK-MIL, GMSK and SOQPSK-TG was found to be 1.15, 0.9 and 2.3 dB respectively.

Table 6.3. Loss in dB for noncoherent systems with phase noise of $\delta = 5°$/sym. at $P_b = 10^{-5}$.

Modulation Scheme	$a = 0.875$	$a = 0.75$	$a = 0.625$
SOQPSK-MIL	∞	6.2	4.1
SOQPSK-TG	∞	∞	9.8
GMSK with $BT = 0.3$	∞	3.05	2.0
GMSK with $BT = 0.25$	∞	3.1	2.85

Table 6.2 summarizes the loss in dB for noncoherent detectors for the more

severe value of $\delta = 5°$/symbol. The loss measured relative to MLSD at $P_b = 10^{-5}$ for SOQPSK-MIL, GMSK and SOQPSK-TG was 4.1, 2.0 and 9.8 dB respectively. Only the GMSK noncoherent detector perfoms satisfactorily, for this case with $a = 0.625$. This implies that as the severity of phase noise increases, a should be chosen to be low, so as to better track phase change.

Chapter 7

Serially Concatenated Systems with Iterative detection

7.1 Introduction

Extensive research has been done in the recent years to design modulation and coding schemes with performance close to the theoretical Shannon capacity limits. Using the same ingredients as turbo codes [7] (convolutional encoders and interleavers), *serially concatenated convolutional codes* have been shown to yield performance comparable and in some cases superior, to turbo codes [6]. In this chapter we investigate the performance of reduced-complexity noncoherent detectors for SOQPSK and GMSK (the reduced complexity designs are used in the CPM soft-input soft-output (SISO) modules) in serially concatenated coded systems with iterative detection.

7.2 System Description

The block diagram of the system is shown in Figure 7.1. This is the system with SOQPSK as the inner code; when GMSK is used as the inner code a precoder would not be needeed and the SOQPSK SISO would be replaced with a GMSK SISO. The information bits a_n are first passed through a convolutional encoder and interleaved.
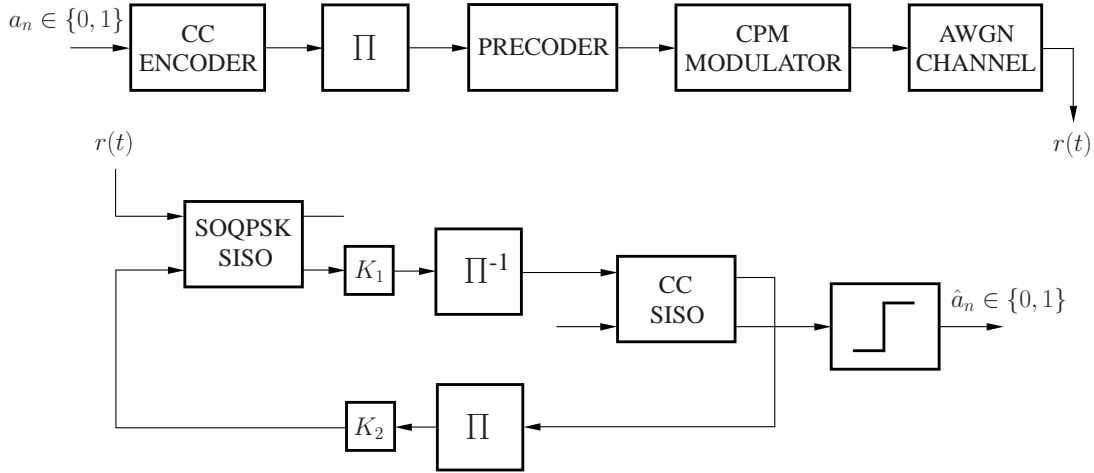
Figure 7.1. Block diagram of serially concatenated system with SO-QPSK as inner code.

The *outer* code is the optimal rate $\frac{1}{2}$, 4-state convolutional code with generator polynomials $g_1 = [1 \ 0 \ 1]$ and $g_2 = [1 \ 1 \ 1]$. This is the same code as was used in [24]. The S-random interleaver [12] (labeled as "Π" in the block diagram) is used to increase the coding gain and improve the overall system performance. The interleaver size should be chosen so as to maximize gain and at the same time not increase decoding complexity and latency by a large factor. The interleaver that we use has $S = 32$ and a block size of $N = 2048$. The interleaved bits are input to the CPM modulator (cascade of the precoder and modulator in case of SOQPSK).

The received signal is demodulated and decoded in an iterative fashion by

soft-input soft-output (SISO) modules from [26] and [5] for CPM and the CC, respectively. These are discussed in more detail later in this chapter. In order to model a practical reduced-complexity implementation, we use "max-log" versions of these SISOs. The soft information exchanged between the two SISOs is in the form of log-likelihood ratios and is scaled by the gains K_1 and K_2 to improve performance [20, 24]. For SOQPSK-MIL we select $K_1 = 0.75$ and $K_2 = 0.75$ [24], and for SOQPSK-TG and GMSK we select $K_1 = 0.8$ and $K_2 = 0.75$. The unconnected CC SISO input in Figure 7.1 is zero, and the lower input to the CPM SISO is initialized to zero for the first iteration. For all simulations in this chapter the number of iterations is $N_{it} = 5$.

7.3 SISO algorithm

The "max-log" version of the SISO algorithm from [5] is briefly summarized here. The SISO module is a four-port device with two inputs and two outputs as shown in Figure 7.2. It accepts as inputs the probability distributions of the information bits $P(a, I)$ and code symbols $P(c, I)$ of the code trellis and outputs $P(a, O)$ and $P(c, O)$ which are the updated versions of these distributions based on the code constraints.
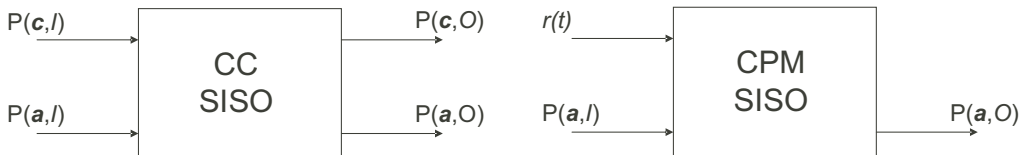
Figure 7.2. The CC and CPM SISO modules.

After the trellis is organized the algorithm makes *forward* and *backward* recursions to update metrics associated with each trellis state and then uses these metrics to compute output probability distributions. The state metrics in the

forward recursion are obtained by

$$A_k(\tilde{E}_k) = A_{k-1}(\tilde{S}_{k-1}) + P_k[\tilde{a}_k; I] + P_k[\tilde{c}_k; I] \tag{7.1}$$

where $k = 1, 2, \cdots, n$. n is the length of the block over which the state metrics are computed. Among the several branches ending at state E_k, the *survivors* (branches having the *maximum* metric) of the path metrics are used for cumulative metric update, which is why the algorithm is referred to as the "max-log" version. This is similar to the VA. The initial condition of $A_0(\cdot) = 0$ is assumed. Likewise, the state metrics for the reverse recursion are obtained by

$$B_k(\tilde{S}_k) = B_{k+1}(\tilde{E}_{k+1}) + P_{k+1}[\tilde{a}_{k+1}; I] + P_{k+1}[\tilde{c}_{k+1}; I] \tag{7.2}$$

where $k = n - 1, \cdots, 0$. The initial condition of $B_n(\cdot) = 0$ is assumed. The output probability distributions $\tilde{P}_k(c^j; O)$ and $\tilde{P}_k(a^j; O)$ for the jth bit within each symbol at time k are computed as

$$P_k(a_k; O) = A_{k-1}(\tilde{S}_{n-1}) + P_k[a^j; I] + P_k[c^j; I] + B_k(\tilde{E}_n). \tag{7.3}$$

Similar to the computation of A and B, there will be several branches which have the same input bit a^j (or code word c^j) and we select the branch which has the highest metric.

7.4 Reduced complexity CPM SISO Module

The CPM SISO is connected in series with the CC SISO, it takes as input the received signal (instead of the probability distribution of code words) and the

input bit probability distribution (from the CC SISO) and outputs the update for the information bit probability distribution based on the CPM trellis.

In order to view CPM as a code, the length-T segments of the waveform are regarded as "codewords." The probability distribution for the codeword is then replaced by

$$P_k[c_k, I] = \text{Re}\{e^{-j\theta_{n-L}} z_k(\tilde{\boldsymbol{\alpha}}_{\boldsymbol{k}})\} \tag{7.4}$$

where $z(\cdot)$ is the sampled matched filter output defined by (3.9).

In case of the noncoherent CPM SISO it metric is be replaced by

$$P_k[c_k, I] = \text{Re}\{Q_n^*(\tilde{S}_n)e^{-j\theta_{n-L}} z_k(\tilde{\boldsymbol{\alpha}}_{\boldsymbol{k}})\} \tag{7.5}$$

where $Q(\cdot)$ is as described in Chapter 5 and updated using (5.3). The update for $Q(\cdot)$ is done only in the forward recursion.

7.5 Performance

In this section we look at the simulation results for coherent and noncoherent coded systems. There are no termination bits added anywhere in the simulations, and the decoder state metrics are initialized to zero for each iteration. It was found in [21] that large coding gains were possible when the number of iterations were increased from 1 to 3, and beyond 5 iterations performance does not significantly improve. More than 5 iterations only add to the system latency and so we chose to have 5 iterations for simulations. The choice of interleaver size of 2048 and 5 iterations allows us to compare the performance of SCC GMSK system to that of SOQPSK-TG in [29].

Figure 7.3 shows the performance of coded SOQPSK and GMSK systems. It

can be observed that the performance of SOQPSK-TG is 0.2 dB inferior to that of SOQPSK-MIL at $P_b = 10^{-5}$ and GMSK with $BT = 0.25$ is 0.06 dB worse when compared to GMSK with $BT = 0.3$. This is obvious as SOQPSK-TG and GMSK with $BT = 0.25$ are more bandwidth efficient than SOQPSK-MIL and GMSK with $BT = 0.3$ respectively and have smaller minimum distance in the uncoded case.
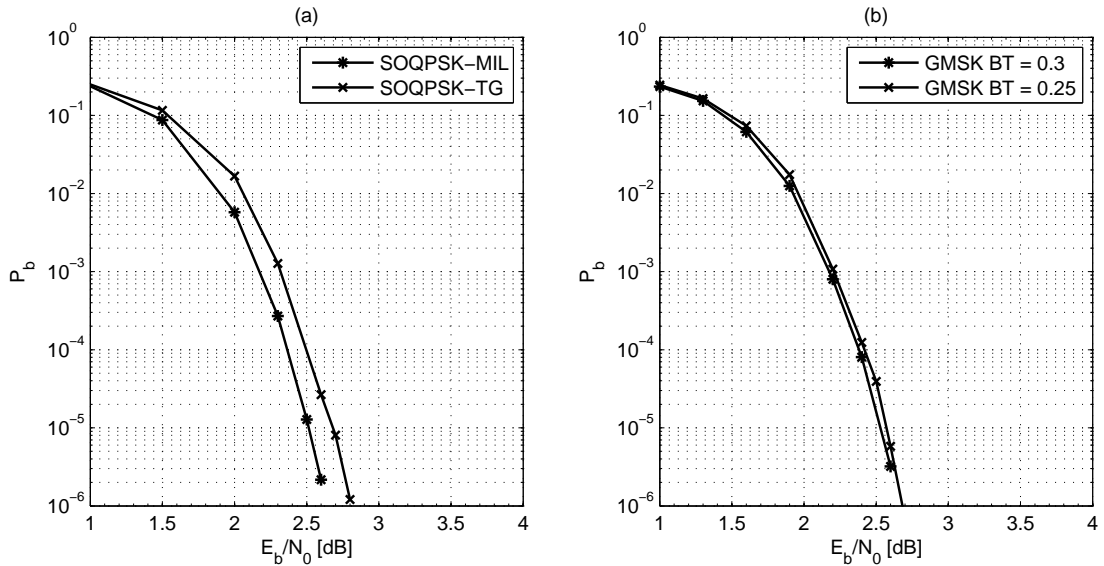
Figure 7.3.   Performance of coded a) SOQPSK and b) GMSK systems.

The gains for each coded configuration are listed in Table 7.1. SOQPSK-TG and GMSK with $BT = 0.25$ have higher coding gain when compared to the less bandwidth efficient schemes. Thus we conclude that more bandwidth-efficient modulation achieves higher gain in coded systems, this conclusion was also reached in [24] for coded SOQPSK.

Figures 7.4 and 7.5 show the performance of noncoherent SOQPSK and GMSK systems with no phase noise. The forgetting factor a was chosen to be 0.875 for all the noncoherent cases. It was found in the previous chapter that this value

Table 7.1. Coding gains for serially concatenated SOQPSK and GMSK.

Modulation Scheme	Gain in dB
SOQPSK-MIL	7.35
SOQPSK-TG	7.72
GMSK with $BT = 0.3$	7.46
GMSK with $BT = 0.25$	7.53

of a is optimum for low to moderate phase noise. Even in severe phase noise we choose a for coded systems to be 0.875 since $\frac{E_b}{N_o}$ is low enough to make thermal noise the dominant impairment.
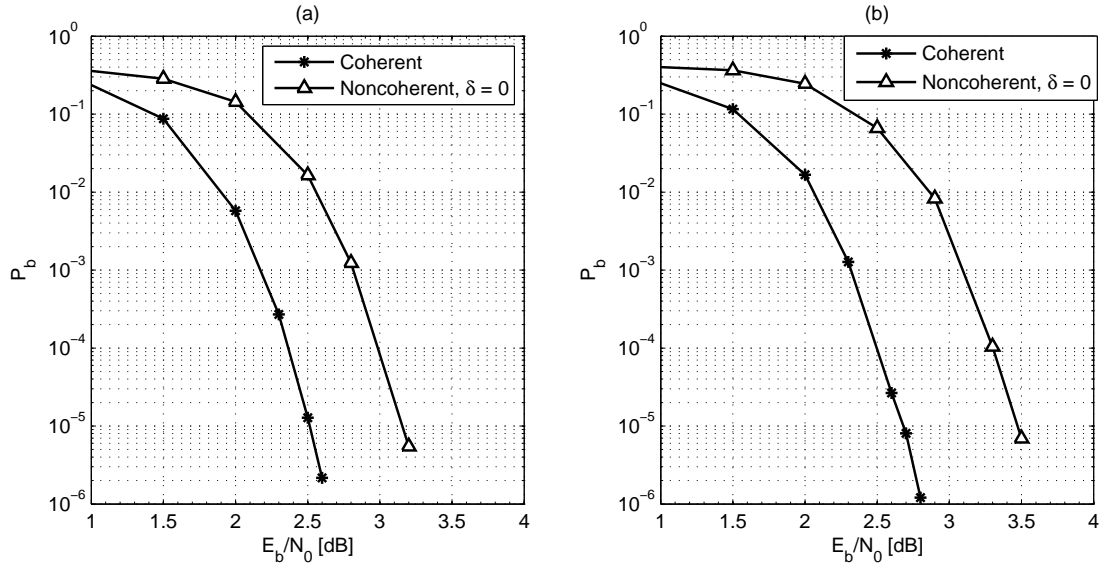
Figure 7.4. Coded noncoherent a) SOQPSK-MIL and b) SOQPSK-TG with no phase noise.

Figures 7.6 through 7.9 show the performance of noncoherent SOQPSK and GMSK systems with phase noise. The phase noise model is the one discussed in section 6.2. As in the previous chapter $\delta = 2°$/symbol and $\delta = 5°$/symbol were the 2 values chosen for δ.

As in the case of uncoded systems, the benchmark for comparing the perfor-
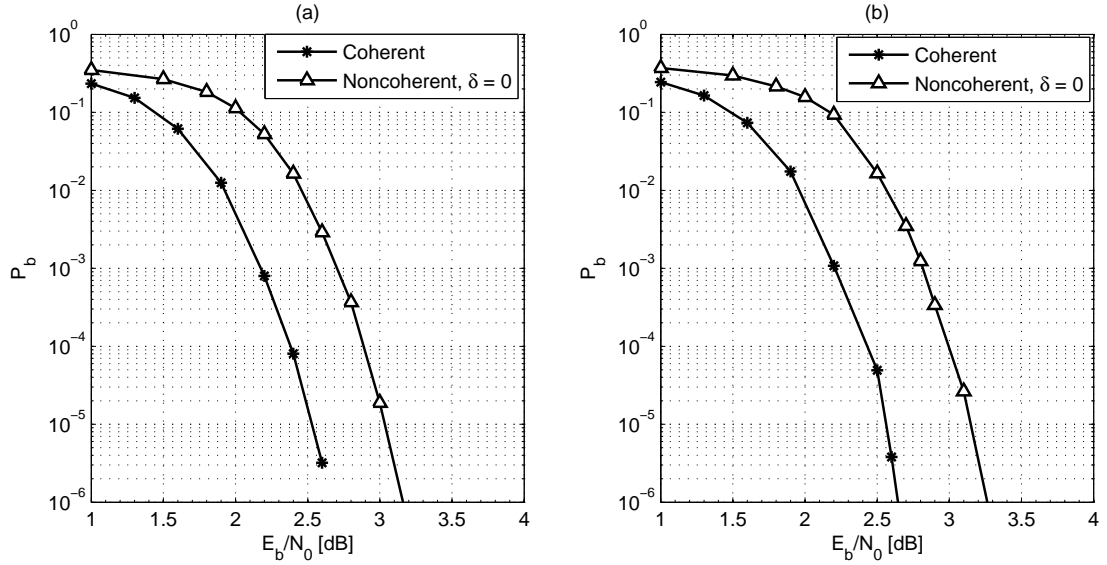
Figure 7.5. Coded noncoherent a) GMSK (BT = 0.3) and b) GMSK (BT = 0.25) with no phase noise.
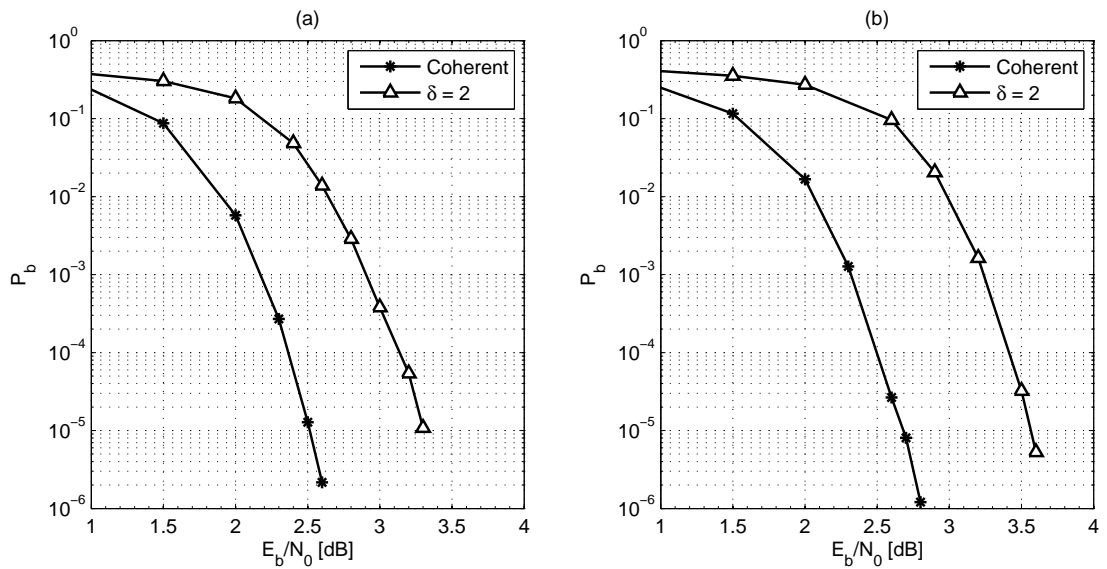
Figure 7.6. Coded noncoherent a) SOQPSK-MIL and b) SOQPSK-TG with $\delta = 2°$ /symbol.
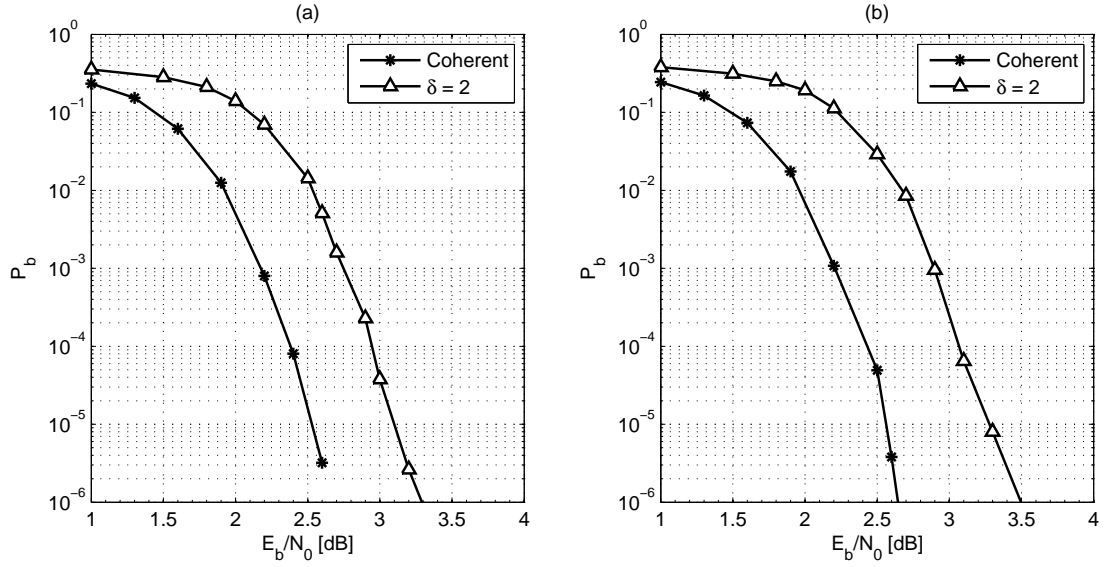
Figure 7.7. Coded noncoherent a) GMSK ($BT = 0.3$) and b) GMSK ($BT = 0.25$) with $\delta = 2°$ /symbol.
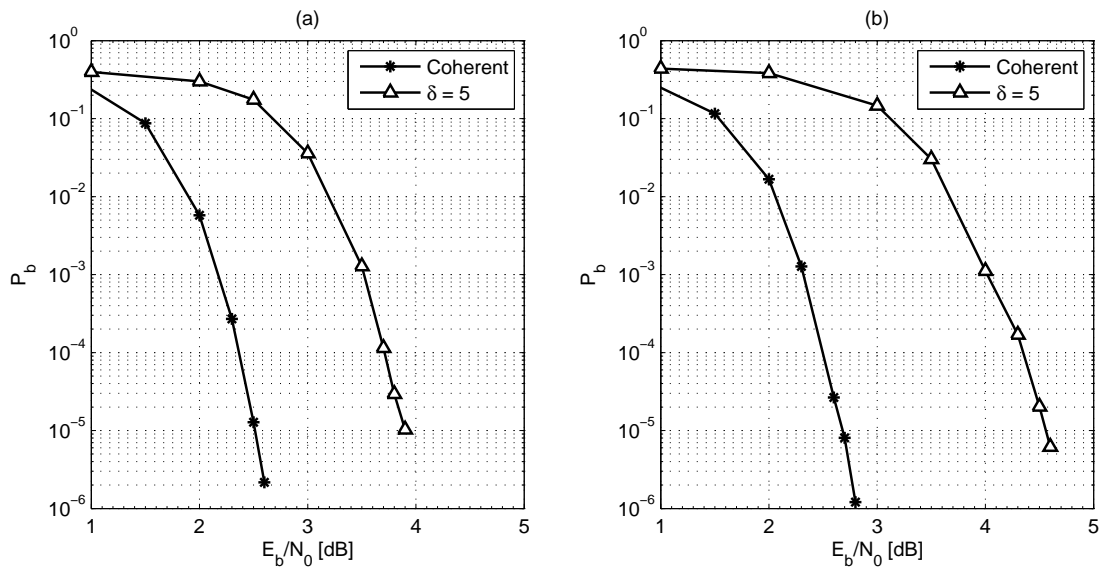
Figure 7.8. Coded noncoherent a) SOQPSK-MIL and b) SOQPSK-TG with $\delta = 5°$ /symbol.
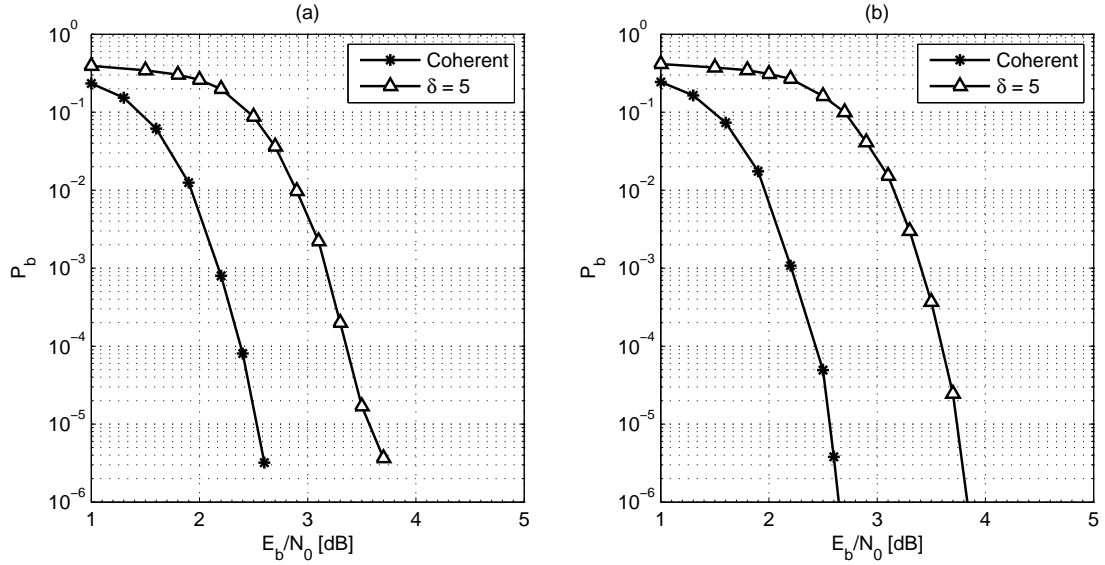
Figure 7.9. Coded noncoherent a) GMSK (BT = 0.3) and b) GMSK ($BT = 0.25$) with $\delta = 5°$ /symbol.

mance of noncoherent detectors is coherent detection. Table 7.2 summarizes loss in dB at $P_b = 10^{-5}$ for noncoherent detectors for different values of δ.

Table 7.2. Loss in dB for noncoherent (coded) systems at $P_b = 10^{-5}$.

Modulation Scheme	$\delta = 0°$/sym.	$\delta = 2°$/sym.	$\delta = 5°$/sym.
SOQPSK-MIL	0.68	0.54	1.40
SOQPSK-TG	0.79	0.71	1.88
GMSK with $BT = 0.3$	0.50	0.55	1.03
GMSK with $BT = 0.25$	0.61	0.71	1.17

It can be seen that the SOQPSK-MIL and GMSK with $BT = 0.3$ have almost identical performance with a moderate phase noise of $\delta = 2$ and GMSK with $BT = 0.3$ is slightly better for the noncoherent case with no phase noise. Also SOQPSK-TG and GMSK with $BT = 0.25$ have identical performance for $\delta = 0°, 2°$.

For the more severe case of phase noise, when $\delta = 5°$, the noncoherent GMSK detectors perform better than noncoherent SOQPSK detectors. GMSK with

$BT = 0.3$ has the best performance with a loss of 1.03 dB with respect to coherent detection. It is clearly the best modulation scheme that can be used for coded noncoherent detection as it has good peformance in cases of moderate to severe phase noise.

Chapter 8

Conclusions

We developed reduced complexity coherent detectors for full response and partial response SOQPSK and GMSK. We proposed a noncoherent detection algortihm which can be used in both uncoded and coded systems with iterative detection and applied it to build noncoherent detectors for these two modulation schemes. We used a popular phase noise model to simulate a channel with varying carrier phase and compared the performance of both noncoherent detectors for coded and uncoded systems. We observed that the peformance of GMSK noncoherent detectors is better overall when compared to SOQPSK noncoherent detectors. The key contributions of this work can be summarized as follows.

8.1 Key Contributions

1. Reduced complexity coherent detectors for GMSK were developed. Pulse truncation and decision feedback were extended to GMSK with $BT = 0.25$ and the reduced complexity detector with 1/8 as many trellis states as the optimal detector was found to peform within 0.01 dB of the optimal coherent

detector.

2. A noncoherent detection algorithm which can be used for uncoded and coded systems was presented and was applied to GMSK. In the uncoded case SOQPSK-TG and GMSK with $BT = 0.25$ (PT) have a degradation of 0.75 dB and for coded systems the loss at $P_b = 10^{-5}$ was 0.69 and 0.71 dB respectively.

3. It was found noncoherent GMSK detectors in uncoded systems perform significantly better than noncoherent SOQPSK detectors in cases of severe phase noise. When the standard deviation δ of phase noise is 5°/symbol, the peformance degradation for GMSK with BT = 0.3 and 0.25 is 2.0 and 2.85 dB respectively whereas for SOQPSK-MIL and TG it is 4.1 and 9.8 dB respectively. In cases of low to moderate phase noise SOQPSK-MIL performs almost as well as GMSK.

4. The reduced complexity techniques were used to build noncoherent detectors for coded systems. Noncoherent SISO modules for SOQSK and GMSK was developed, in coded systems it was found that the performance of noncoherent detectors for SOQPSK and GMSK in low to moderate phase noise is almost identical (loss of 0.55 dB for SOQPSK MIL and GMSK with $BT = 0.3$, loss of 0.71 dB for SOQPSK-TG and GMSK with $BT = 0.25$). For severe phase noise, GMSK performs slightly better in coded systems (loss of 1.40 dB for SOQPSK-MIL and 1.03 for GMSK $BT = 0.3$).

8.2 Future Work

We investigated the performance of noncoherent coded systems with a rate $\frac{1}{2}$ convolutional code with generator polynomials $g_1 = [1\ 0\ 1]$ and $g_2 = [1\ 1\ 1]$ as they are widely used. SOQPSK and GMSK performance with other convolutional codes as *outer codes* should be studied in future. Even more bandwidth efficient GMSK schemes (with lower values of BT) could be investigated.

Other reduced complexity techniques such as the PAM decomposition have not been applied to GMSK so far and it is an area for future work.

References

[1] D. I. S. Agency. Department of Defense interface standard, interoperability standard for single-access 5-kHz and 25-kHz UHF satellite communications channels. Tech. Rep. MIL-STD-188-181B, Department of Defense, March 1999.

[2] N. Al-Dhahir and G. Saulnier. A high-performance reduced-complexity GMSK demodulator. *IEEE Trans. Commun.*, 46:1409–1412, Jan. 1998.

[3] J. B. Anderson, T. Aulin, and C.-E. Sundberg. *Digital Phase Modulation*. Plenum Press, New York, 1986.

[4] T. Aulin, C.-E. Sundberg, and A. Svensson. Viterbi detectors with reduced complexity for partial response continuous phase modulation. In *Proc. National Telecommun. Conf., NTC'81*, pages A7.6.1–A7.6.7, New Orleans, LA, Nov./Dec. 1981.

[5] S. Benedetto, D. Divsalar, G. Montorsi, and F. Pollara. A soft-input soft-output APP module for iterative decoding of concatenated codes. *IEEE Commun. Lett.*, 1:22–24, Jan. 1997.

[6] S. Benedetto, D. Divsalar, G. Montorsi, and F. Pollara. Serial concatenation of interleaved codes: Performance analysis, design, and iterative decoding. *IEEE Trans. Inform. Theory*, 44:909–926, May 1998.

[7] C. Berrou, A. Glavieux, and P. Thitimajshima. Near shannon limit error-correcting coding and decoding: Turbo codes. In *Proc. IEEE Int. Conf. Communications*, pages 1064–1070, Geneva, Switzerland, May 1993.

[8] G. Colavolpe, G. Ferrari, and R. Raheli. Noncoherent iterative (turbo) decoding. *IEEE Trans. Commun.*, 48(9):1488–1498, Sept. 2000.

[9] G. Colavolpe, G. Ferrari, and R. Raheli. Reduced-state BCJR-type algorithms. *IEEE J. Select. Areas Commun.*, 19:848–849, May 2001.

[10] G. Colavolpe and R. Raheli. Noncoherent sequence detection. *IEEE Trans. Commun.*, 47(9):1376–1385, Sept. 1999.

[11] M. J. Dapper and T. J. Hill. SBPSK: A robust bandwidth-efficient modulation for hard-limited channels. In *Proc. IEEE MILCOM*, Oct. 1984.

[12] D. Divsalar and F. Pollara, (1995, May). Multiple turbo codes for deep-space communications. *Telecommunications and Data Acquisition Progress Report*, [Online]. Available: http://tmo.jpl.nasa.gov/tmo/progress_report/42-121/121T.pdf.

[13] B. Dural and J. G. Proakis. Signal space representation of binary continuous phase modulated signals. *IEEE Trans. on Vehicular Technology*, 3:1663–1667, October 2001.

[14] M. V. Eyuboglu and S. U. Qureshi. Reduced-state sequence esti mation with set partitioning and decision feedback. *IEEE Trans. Commun.*, 36(1):13–20, Jan. 1988.

[15] R. Fantacci. Proposal of an interference cancellation receiver with low complexity for DS /CDMA mobile communication systems. *IEEE Trans. on Vehicular Technology*, 48(4):1039–1046, July 1999.

[16] K. Feher. Modems for emerging digital cellular-mobile radio system. *IEEE Trans. on Vehicular Technology*, 40:355–365, May 1991.

[17] T. Hill. A non-proprietary, constant envelope, variant of shaped offset QPSK (SOQPSK) for improved spectral containment and detection efficiency. In *Proc. IEEE MILCOM*, Oct. 2000.

[18] M. K. Howlader and X. Luo. Noncoherent iterative demodulation and decoding of serially concatenated coded MSK. In *Proc. IEEE Global Telecommunications Conf.*, volume 2, pages 785–789, Nov./Dec. 2004.

[19] J. Huber and W. Liu. An alternate approach to reduced complexity CPM receivers. *IEEE J. Select. Areas Commun.*, 7:1437–1449, Dec. 1989.

[20] D. Kim, T. Kwon, J. Choi, and J. Kong. A modified two-step SOVA-based turbo decoder with a fixed scaling factor. In *Proc. IEEE Int. Symp. Circuits Syst.*, May 2000.

[21] D. Kumaraswamy. *Simplified Detection Techniques for Serially Concatenated Coded Continuous Phase Modulations*. Masters dissertation, University of Kansas, Lawrence, Kansas, Jul. 2007.

[22] L. Lampe, R. Schober, and M. Jain. Noncoherent sequence detection receiver for Bluetooth systems. *IEEE J. Select. Areas Commun.*, 23(9):1718–1727, Sept. 2005.

[23] P. A. Laurent. Exact and approximate construction of digital phase modulations by superposition of amplitude modulated pulses (AMP). *IEEE Trans. Commun.*, 34:150–160, Feb. 1986.

[24] L. Li and M. Simon. Performance of coded OQPSK and MIL-STD SOQPSK with iterative decoding. *IEEE Trans. Commun.*, 52:1890–1900, Nov. 2004.

[25] G. L. Lui, K. Tsai, Y. Zohng, S. Dolinar, and K. Andrews. Codeed performance of a quaternary GMSK communication system. In *Proc. IEEE MILCOM*, volume 1, pages 36–40, Oct. 2003.

[26] P. Moqvist and T. Aulin. Serially concatenated continuous phase modulation with iterative decoding. *IEEE Trans. Commun.*, 49:1901–1915, Nov. 2001.

[27] E. Perrins. *Reduced Complexity Detection Methods for Continuous Phase Modulation*. Ph.D. dissertation, Brigham Young University, Provo, Utah, Aug. 2005.

[28] E. Perrins, T. Nelson, and M. Rice. Coded FQPSK and SOQPSK with iterative detection. In *Proc. IEEE MILCOM*, Atlantic City, NJ, Oct. 2005.

[29] E. Perrins and M. Rice. Reduced-complexity approach to iterative detection of SOQPSK. *IEEE Trans. Commun.*, 55(7):1354–1362, July 2007.

[30] Range Commanders Council Telemetry Group, Range Commanders Council, White Sands Missile Range, New Mexico. *IRIG Standard 106-00: Telemetry Standards*, 2000. (Available on-line at http://www.ntia.doc.gov/osmhome/106.pdf).

[31] D. Raphaeli and D. Divsalar. Noncoherent detection of continuous phase modulation using

overlapped observations. In *Proc. IEEE Global Telecommunications Conf.*, pages 191–195, Nov. 1994.

[32] R. Rhodes, S. Wilson, and A. Svensson. MSK-type reception of continuous phase modulation: Cochannel and adjacent channel interference. *IEEE Trans. Commun.*, 35:185–193, Feb. 1987.

[33] B. E. Rimoldi. A decomposition approach to CPM. *IEEE Trans. Inform. Theory*, 34:260–270, Mar. 1988.

[34] R. Schober and W. H. Gerstacker. Metric for noncoherent sequence estimation. *Electron. Lett.*, 35(25):2178–2179, Dec. 1999.

[35] M. R. Shane and R. D. Wesel. Reduced complexity iterative demodulation and decoding of serial concatenated continuous phase modulation. In *Proc. IEEE Int. Conf. Communications*, volume 3, pages 1672–1676, Apr./May 2002.

[36] S. J. Simmons. Simplified coherent detection of CPM. *IEEE Trans. Commun.*, 43:726–728, Feb./Mar./Apr. 1995.

[37] S. J. Simmons and P. H. Wittke. Low complexity decoders for constant envelope digital modulations. *IEEE Trans. Commun.*, 31:1273–1280, Dec. 1983.

[38] M. Simon. *Bandwidth-Efficient Digital Modulation With Application to Deep-Space Communication*. Wiley, New York, 2003.

[39] B. Sklar. *Digital Communications*. Prentice Hall, New York, 2001.

[40] R. Steele. *Mobile Radio Communication*. Pentech, New York, 1995.

[41] A. Svensson. Reduced state sequence detection of partial response continuous phase modulation. *IEE Proc., pt. I*, 138:256–268, Aug. 1991.

[42] A. Svensson, C.-E. Sundberg, and T. Aulin. A class of reduced-complexity Viterbi detectors for partial response continuous phase modulation. *IEEE Trans. Commun.*, 32:1079–1087, Oct. 1984.

[43] W. Tang and E. Shwedyk. A quasi-optimum receiver for continuous phase modulation. *IEEE Trans. Commun.*, 48:1087–1090, July 2000.

[44] J. Wu and G. Saulnier. A two-stage MSK-type detector for Low-BT GMSK signals. *IEEE Trans. on Vehicular Technology*, 52(4), July 2003.